JOURNAL OF AIRCRAFT
Vol. 36, No. 5, September–October 1999

Nonlinear Equivalent Plate Modeling of Wing-Box Structures

Eli Livne* and Israel Navarro†
University of Washington, Seattle, Washington 98195-2400

A geometrically nonlinear moderate-deformation equivalent plate modeling capability for wing structures is developed. It is a generalization of the simple-polynomial-based equivalent plate modeling techniques for linear wing structures. The formulation allows first-order shear deformation plate theory or classical plate theory to be used for modeling and solid thin plates as well as typical wing-box structures made of cover skins and an array of spars and ribs. Mass and stiffness matrix contributions of different wing-box elements are presented. Stiff springs are included to enforce a variety of boundary conditions. The resulting nonlinear equations can be solved for static and dynamic structural response. The new nonlinear equivalent plate modeling technique was validated by comparing its results with those of nonlinear finite element models and results of previous analyses. It is expected to lead to efficient nonlinear aeroelastic analysis of wings subject to in-plane compressive forces such as the rear wings in joined-wing airplane configurations.

Nomenclature

$\{\boldsymbol{a}_1(x, y)\} - \{\boldsymbol{a}_5(x, y)\}$	= Ritz function vectors in Eqs. (18–22)
$c\Lambda$	= cos Λ
$\{\boldsymbol{Fr}_x\}$, $\{\boldsymbol{Fr}_y\}$, $\{\boldsymbol{Fr}_z\}$	= coefficients of distributed external force polynomials
$(\hat{F}r_x, \hat{F}r_y, \hat{F}r_z)$	= components of a concentrated force at a point
$H(g)$	= series coefficients in a depth polynomial series; Eq. (9)
$h_U(x, y)$, $h_L(x, y)$	= z positions of upper and lower skins, respectively
$I_{\mathrm{SP}}(r, s)$	= family of line integrals for a spar
$I_{\mathrm{TR}}(r, s)$	= family of area integrals for a skin trapezoid
$[K]$	= matrix defined by $U = \frac{1}{2}\{\boldsymbol{q}\}^T[K(\{\boldsymbol{q}\})]\{\boldsymbol{q}\}$
$[\bar{K}]$	= stiffness matrix
$[K_L]$	= linear part of $[K]$ matrix
$[K_{\mathrm{NL}}]$	= nonlinear part of the $[K]$ matrix
$[K_{\mathrm{NL},q(j)}]$	= $\partial K_{\mathrm{NL}} \div [\partial q(j)]$
$[K_S]$	= see Eq. (79)
k_u, k_v, k_w	= spring coefficients for stiff springs
$[M]$	= mass matrices
$mfrx(i)$, $mfry(i)$, $mfrz(i)$	= powers of x terms in polynomial series representing distributed loads
$mh(g)$, $nh(g)$	= powers of x and y terms in a depth polynomial series; Eq. (9)
$mt(k)$, $nt(k)$	= powers of x and y terms in the polynomial series for skin-layer thickness; Eq. (10)
$mu(i)$, $nu(i)$	= powers of polynomial terms in the series for $u_0(x, y, t)$
$mv(i)$, $nv(i)$	= powers of polynomial terms in the series for $v_0(x, y, t)$
$mw(i)$, $nw(i)$	= powers of polynomial terms in the series for $w_0(x, y, t)$
$m\phi_x(i)$, $n\phi_x(i)$	= powers of polynomial terms in the series for $\phi_x(x, y, t)$
$m\phi_y(i)$, $n\phi_y(i)$	= powers of polynomial terms in the series for $\phi_y(x, y, t)$
$Ntrb$	= number of terms in rib-web-thickness series
$Ntsw$	= number of terms in spar-web-thickness series
Ntt	= number of terms in skin-thickness series
$N_{q\mathrm{tot}}$	= total number of degrees of freedom
N_{tu}, N_{tv}, N_{tw}, $N_{t\phi x}$, $N_{t\phi y}$	= number of terms in Ritz polynomial series for displacement fields; Eqs. (13–17)
$nfrx(i)$, $nfry(i)$, $nfrz(i)$	= powers of y terms in polynomial series representing distributed loads
$\{\boldsymbol{P}\}$	= vector of generalized forces
$\{\boldsymbol{q}\}$	= vector of unknown generalized displacements
$q1(i)$, $q2(i)$, $q3(i)$, $q4(i)$, $q5(i)$	= generalized displacements; Eqs. (13–17)
$\{\boldsymbol{R}_e\}$	= vector of elastic forces
$s\Lambda$	= sin Λ
T	= kinetic energy
$T(k)$	= coefficients in the polynomial series for skin-layer thickness; Eq. (10)
$T_{rb}(k)$	= coefficients in the polynomial series for rib-web-layer thickness
$t_{rb}(x)$	= thickness of a layer in a rib web
$T_{sw}(k)$	= coefficients in the polynomial series for spar-web-layer thickness
$t_{sw}(y)$	= thickness of a layer in a spar web
T_u, T_v, T_w	= kinetic energies due to motion in the x, y, and z directions, respectively
$t(x, y)$	= thickness of skin layer
U	= elastic potential energy
u, v, w	= displacements in the x, y, and z directions, respectively (functions of x, y, z, and t)
$u_{,x}$	= $\partial u/\partial x$
u_0, v_0, w_0	= x, y, z displacements of a reference surface (functions of x, y, and t)
$v_{,y}$	= $\partial v/\partial y$
$w_{,x}$	= $\partial w/\partial x$
$w_{,xx}$, $w_{,yy}$, $w_{,xy}$	= $\partial^2 w/\partial^2 x$, $\partial^2 w/\partial^2 y$, and $\partial^2 w/\partial x\partial y$, respectively
$w_{,y}$	= $\partial w/\partial y$
$w_{,z}$	= $\partial w/\partial z$
xa, ya	= point of application of a concentrated force

Received 1 April 1998; revision received 10 December 1998; accepted for publication 9 January 1999.

*Associate Professor, Department of Aeronautics and Astronautics. Associate Fellow AIAA.
†Graduate Student, Department of Aeronautics and Astronautics.

xsp, ysp = coordinates of a spring-point location
x_{rbA}, x_{rbF} = aft and front tips of a rib line; Eq. (96)
y_L, y_R, x_{FL}, x_{FR}, x_{AR}, x_{AL} = (x, y) coordinates of the vertices defining a planform trapezoid; Fig. 1
y_{RIB} = y coordinate of a rib line
γ_{xz}, γ_{yz} = transverse shear strains
ε_{ij} = strains
Λ = sweep angle of a spar line with respect to the y axis
ρ = material density
$\phi_{,x}$ = $\partial\phi/\partial x$
ϕ_x, ϕ_y = first-order shear rotation corrections to the classical plate theory rotation [Eq. (3)], functions of x, y, and t
$\phi_{,y}$ = $\partial\phi/\partial y$
Ψ_x, Ψ_y = first-order transverse shear rotations [Eq. (2)], functions of x, y, and t

Subscripts

d = displacement (linear) spring
rb = rib
rt = rotational spring
sp = spar

Introduction

THE emergence of optimized lightweight highly maneuverable unmanned combat air vehicles (UCAVs), capable of performing very-high-g maneuvers, as well as the need for further design evaluation of the joined wing,[1,2] a configuration in which a long and quite large tail surface is under significant compression, calls for the development of efficient structural analysis and design techniques for the aeroelastic studies of geometrically nonlinear lifting surfaces.

While detailed finite element models for linear and nonlinear analysis of airplane structures[3] are now well established and are general in their capacity to capture behavior of local nature as well as global behavior (depending on the fineness of the mesh used), they lead to large-scale mathematical models that are expensive to generate and solve. This is particularly true in the context of design optimization, where many function evaluations are required. Equivalent plate structural models representing real airplane wings were developed during the past 15 years[4–15] and were found to be accurate and computationally effective. Initially, these models were based on classical plate theory (CPT).[16] They later were improved to include transverse shear deformation effects.[10,11,13] The experience gained with the resulting equivalent plate linear structural wing analysis based on first-order shear deformation plate theory (FSDPT) shows that this modeling approach captures accurately the static and dynamic behavior of both high-aspect ratio and low-aspect ratio multispar/multirib thin or thick wings.

In an effort to develop design-oriented structural analysis for geometrically nonlinear elastic wings, such as thin optimized wings for very high-g unmanned airplanes, or wings subjected to in-plane compression, as can be found in joined wings, the approach taken in the present study is to extend FSDPT equivalent plate wing modeling from linear to geometrically nonlinear analysis.

This paper discusses the application of nonlinear plate theory and simple-polynomial Ritz approximations to real wing structures (including their cover skins, spar and rib caps, and spar and rib webs). The dynamic equations of motion are formulated. Solutions of the static and dynamic problems are discussed. Test cases and test results are used to assess the accuracy of the resulting capability, and this paper concludes with lessons learned and recommendations for future research.

Kinematic Assumptions in CPT and FSDPT

For a thin plate in the x–y plane, CPT is based on the assumption that deformations can be approximated in the following form [where $u(x, y, z, t)$; $v(x, y, z, t)$; and $w(x, y, z, t)$ are the displacements in the x, y, and z directions, respectively]:

$$u(x, y, z, t) = u_0(x, y, t) - zw_{,x}(x, y, t)$$
$$v(x, y, z, t) = v_0(x, y, t) - zw_{,y}(x, y, t)$$
$$w(x, y, z, t) = w_0(x, y, t) \tag{1}$$

The x, y-dependent displacement functions u_0, v_0, and w_0 are the values of u, v, and w at the reference plane ($z = 0$); and u_0 and v_0 represent the stretching of the midplane.

The most common formulation of kinematic assumptions in the FSDPT is[10,16,17]

$$u(x, y, z, t) = u_0(x, y, t) - z\Psi_x(x, y, t)$$
$$v(x, y, z, t) = v_0(x, y, t) - z\Psi_y(x, y, t)$$
$$w(x, y, z, t) = w_0(x, y, t) \tag{2}$$

Here, the x, y-dependent functions Ψ_x and Ψ_y augment the deformation functions used in Eq. (1), leading to five different unknown functions: $u_0(x, y, t)$, $v_0(x, y, t)$, $w_0(x, y, t)$, $\Psi_x(x, y, t)$, and $\Psi_y(x, y, t)$ for the deformation field of the plate. References 10 and 13 showed how the kinematic assumptions of Eq. (2) can be used to include transverse shear deformation effects in the equivalent plate modeling of wing-box structures. Developments described in Ref. 13 led to an equivalent plate capability where wing segments in which transverse shear cannot be neglected [Eq. (2)] are combined with a wing segment modeled using CPT [Eq. (1)] for the modeling of wing-box/control-surface configurations. In the formulation behind the capability of Ref. 13, the wing is divided into zones, where a zone is a wing segment for which displacements are approximated by its own set of Ritz functions. Thus, a CPT zone has its own Ritz functions for the u_0, v_0, and w_0 deformations; and a FSDPT zone has its own Ritz functions for its own $u_0(x, y, t)$, $v_0(x, y, t)$, $w_0(x, y, t)$, $\Psi_x(x, y, t)$, and $\Psi_y(x, y, t)$ deformations. Formulations of stiffness and mass matrices for CPT and FSDPT zones are different and separate.

In an effort to develop a single formulation for CPT and FSDPT zones, Ref. 14 presents the kinematic plate assumptions in the following form:

$$u(x, y, z, t) = u_0(x, y, t) - z[w_{,x}(x, y, t) - \phi_x(x, y, t)]$$
$$v(x, y, z, t) = v_0(x, y, t) - z[w_{,y}(x, y, t) - \phi_y(x, y, t)]$$
$$w(x, y, z, t) = w_0(x, y, t) \tag{3}$$

The rotation of cross sections in Eq. (3) is made of a CPT rotation [Eq. (1)] plus a corrective rotation due to transverse shear in the form of the functions ϕ_x and ϕ_y. A single formulation can now be used because a CPT zone is obtained by simply setting the ϕ_x and ϕ_y contributions to zero. Comparing Eqs. (2) and (3), it becomes clear that

$$\Psi_x = w_{,x} - \phi_x, \qquad \Psi_y = w_{,y} - \phi_y \tag{4}$$

Actually, it can be shown that ϕ_x and ϕ_y are the transverse shear strains γ_{xz} and γ_{yz}.

Having established Eq. (3) as the basis of the displacement assumptions to be used in the present work, strains can now be expressed in terms of the unknown displacement functions as follows, based on conventional moderately nonlinear plate theory[17–19]:

$$\varepsilon_{xx} = u_{,x} + \tfrac{1}{2}(w_{,x})^2, \qquad \varepsilon_{yy} = v_{,y} + \tfrac{1}{2}(w_{,y})^2$$
$$\varepsilon_{zz} = w_{,z} + \tfrac{1}{2}(w_{,z})^2, \qquad \varepsilon_{xy} = \tfrac{1}{2}(u_{,y} + v_{,x} + w_{,x}w_{,y})$$
$$\varepsilon_{xz} = \tfrac{1}{2}(u_{,z} + w_{,x} + w_{,x}w_{,z}), \qquad \varepsilon_{yz} = \tfrac{1}{2}(v_{,z} + w_{,y} + w_{,y}w_{,z}) \tag{5}$$

Substituting Eq. (3) into Eq. (5) leads to

$$\varepsilon_{xx} = u_{0,x} - zw_{0,xx} + z\phi_{x,x} + \tfrac{1}{2}(w_{0,x})^2$$

$$\varepsilon_{yy} = v_{0,y} - zw_{0,yy} + z\phi_{y,y} + \tfrac{1}{2}(w_{0,y})^2, \qquad \varepsilon_{zz} = 0$$

$$\varepsilon_{xy} = \tfrac{1}{2}[u_{0,y} + v_{0,x} - 2zw_{0,xy} + z(\phi_{x,y} + \phi_{y,x}) + w_{0,x}w_{0,y}]$$

$$\varepsilon_{xz} = \tfrac{1}{2}\phi_x, \qquad \varepsilon_{yz} = \tfrac{1}{2}\phi_y \tag{6}$$

Effects of Initial Displacements

Initial imperfections, in the form of an initial stress-free shape $w_I(x, y)$, can have significant effects in nonlinear analysis of plates.[17,18] Neglecting high-order terms, the equations of strains in the presence of initial plate imperfections are[17,18]

$$\varepsilon_{xx} = u_{,x} + w_{I,x}w_{,x} + \tfrac{1}{2}(w_{,x})^2$$

$$\varepsilon_{yy} = v_{,y} + w_{I,y}w_{,y} + \tfrac{1}{2}(w_{,y})^2, \qquad \varepsilon_{zz} = 0$$

$$\varepsilon_{xy} = \tfrac{1}{2}(u_{,y} + v_{,x} + w_{I,x}w_{,y} + w_{I,y}w_{,x} + w_{,x}w_{,y})$$

$$\varepsilon_{xz} = \tfrac{1}{2}(u_{,z} + w_{,x}), \qquad \varepsilon_{yz} = \tfrac{1}{2}(v_{,z} + w_{,y}) \tag{7}$$

In terms of the five unknown FSDPT displacement functions $u_0(x, y, t)$, $v_0(x, y, t)$, $w_0(x, y, t)$, $\phi_x(x, y, t)$, and $\phi_y(x, y, t)$, the strains are

$$\varepsilon_{xx} = u_{0,x} - zw_{0,xx} + z\phi_{x,x} + w_{I,x}w_{0,x} + \tfrac{1}{2}(w_{0,x})^2$$

$$\varepsilon_{yy} = v_{0,y} - zw_{0,yy} + z\phi_{y,y} + w_{I,y}w_{0,y} + \tfrac{1}{2}(w_{0,y})^2$$

$$\varepsilon_{xy} = \tfrac{1}{2}[u_{0,y} + v_{0,x} - 2zw_{0,xy} + z(\phi_{x,y} + \phi_{y,x}) + w_{I,x}w_{0,y} + w_{I,y}w_{0,x} + w_{0,x}w_{0,y}]$$

$$\varepsilon_{xz} = \tfrac{1}{2}\phi_x, \qquad \varepsilon_{yz} = \tfrac{1}{2}\phi_y, \qquad \varepsilon_{zz} = 0 \tag{8}$$

Wing-Box Modeling

The kinematic assumptions of the previous section can be used to derive equations of motion for both solid plates and built-up wing-box structures. In the case of built-up wing-box structures, there should be no confusion due to the fact that kinematic plate assumptions are used. Although plate theory is used in this case, the structure modeled is not a solid plate, but, rather, a wing structure made of composite cover skins and an internal array of spar and rib webs. Spar caps and rib caps can, in this formulation, be derived independently, or modeled as smeared equivalent composite skin layers.[13,14]

The wing is defined with respect to a right-handed Cartesian coordinate system as shown in Fig. 1. The reference surface is the x–y plane ($z = 0$). The planform of a wing segment is assumed to have a trapezoidal shape, with the left and right sides parallel to the x axis, and the spanwise direction in the direction of the y axis. Six variables are used to define the planform: y_L, y_R, x_{FL}, x_{FR}, x_{AR}, and x_{AL}, where the variables y_L, and y_R define the left and right sides of the planform, respectively; the variables x_{FL} and x_{FR} define the front-left and front-right corners of the panel, respectively; and x_{AL} and x_{AR} define the aft-left and aft-right corners, respectively. Different or equal trapezoidal areas can be used for the upper and lower surfaces of the box. The location of the spars is determined by defining their left and right endpoints (sx_L, sy_L) and (sx_R, sy_R). Ribs are set parallel to the x axis, and their spanwise location y_{RIB} defines their position. Ribs are assumed to connect the front and aft lines of the trapezoid on which they are located.

In a modeling and solution formulation based on simple polynomials, the depth of a wing segment, as well as thicknesses of skin and web fiber composite layers, are all defined mathematically using simple polynomials. Depth is taken into account by defining the z position of cover skins, using different polynomial series for the upper and lower skins:

$$h(x, y) = \sum_{g=1}^{Nth} H(g) \cdot x^{mh(g)} \cdot y^{nh(g)} \tag{9}$$

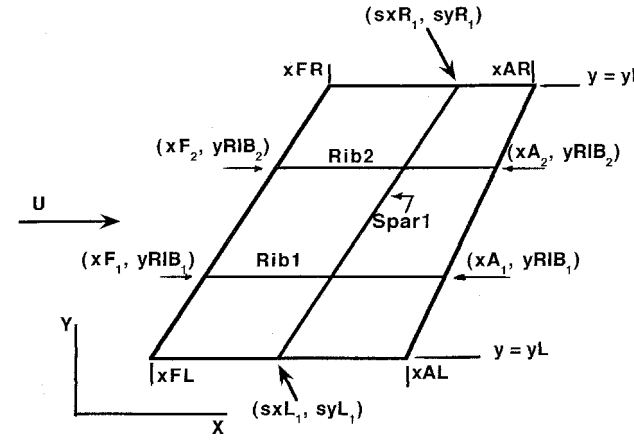

Fig. 1 Planform geometry of wing trapezoids, spars, and ribs.

The coefficients $H(g)$ and the set of powers chosen $mh(g)$ and $nh(g)$ are generated by the analyst to approximate with the best possible accuracy the actual z location of the upper (or lower) skin. An upper depth distribution $h_U(x, y)$ and lower depth distribution $h_L(x, y)$ are needed for each wing trapezoid. Skin layers, in the case of a typical wing box, are considered very thin compared with the depth, and all skin layers are assumed to be at the same z position. The individual thickness of each skin layer is modeled independently by a polynomial series:

$$t(x, y) = \sum_{k=1}^{Ntt} T(k) \cdot x^{mt(k)} \cdot y^{nt(k)} \tag{10}$$

with coefficients $T(k)$ and powers $mt(k)$ and $nt(k)$. When spar webs are modeled, the thickness of each layer can be expressed as a polynomial in y along the spar line (assuming no variation in the z direction):

$$t_{sw}(y) = \sum_{k=1}^{Ntsw} T_{sw}(k) \cdot y^{ntsw(k)} \tag{11}$$

For rib webs, the thickness distribution of composite layers is given by a polynomial series in x along the rib line:

$$t_{rb}(x) = \sum_{k=1}^{Ntrb} T_{rb}(k) \cdot x^{ntrb(k)} \tag{12}$$

Unknown Displacement Functions and Their Ritz Polynomial Series

All unknown functions describing the displacements of the wing box are expressed in terms of simple polynomial series with unknown coefficients:

$$u_0(x, y, t) = \sum_{i=1}^{N_{tu}} q1(i) \cdot x^{mu(i)} \cdot y^{nu(i)} \tag{13}$$

$$v_0(x, y, t) = \sum_{i=1}^{N_{tv}} q2(i) \cdot x^{mv(i)} \cdot y^{nv(i)} \tag{14}$$

$$w_0(x, y, t) = \sum_{i=1}^{N_{tw}} q3(i) \cdot x^{mw(i)} \cdot y^{nw(i)} \tag{15}$$

$$\phi_x(x, y, t) = \sum_{i=1}^{N_{t\phi x}} q4(i) \cdot x^{m\phi x(i)} \cdot y^{n\phi x(i)} \tag{16}$$

$$\phi_y(x, y, t) = \sum_{i=1}^{N_{t\phi y}} q5(i) \cdot x^{m\phi y(i)} \cdot y^{n\phi y(i)} \tag{17}$$

The powers $mu(i)$, $nu(i)$, $mv(i)$, $nv(i)$, etc., in Eqs. (13–17) are chosen in advance, usually using complete polynomials up to a certain order. The choice of polynomials can also be done so that they satisfy automatically certain boundary conditions. Otherwise, stiff springs are used to impose boundary conditions.[7,8,11,13,14] The integers N_{tu}, N_{tv}, N_{tw}, $N_{t\phi x}$, and $N_{t\phi y}$ are the numbers of terms used to expand the functions $u_0(x, y)$, $v_0(x, y)$, $w_0(x, y)$, $\phi_x(x, y)$, and $\phi_y(x, y)$, respectively, in simple polynomial series. These values will determine the size of the mass and stiffness matrices. Time dependence is found in the generalized displacements themselves in the vectors $\{\boldsymbol{q}1(t)\}$, $\{\boldsymbol{q}2(t)\}$, $\{\boldsymbol{q}3(t)\}$, $\{\boldsymbol{q}4(t)\}$, and $\{\boldsymbol{q}5(t)\}$.

In vector form, Eqs. (13–17) are

$$u_0(x, y, t) = \{\boldsymbol{a}_1(x, y)\}^T \cdot \{\boldsymbol{q}1(t)\} \tag{18}$$

$$v_0(x, y, t) = \{\boldsymbol{a}_2(x, y)\}^T \cdot \{\boldsymbol{q}2(t)\} \tag{19}$$

$$w_0(x, y, t) = \{\boldsymbol{a}_3(x, y)\}^T \cdot \{\boldsymbol{q}3(t)\} \tag{20}$$

$$\phi_x(x, y, t) = \{\boldsymbol{a}_4(x, y)\}^T \cdot \{\boldsymbol{q}4(t)\} \tag{21}$$

$$\phi_y(x, y, t) = \{\boldsymbol{a}_5(x, y)\}^T \cdot \{\boldsymbol{q}5(t)\} \tag{22}$$

where $\{\boldsymbol{a}_1(x, y)\} - \{\boldsymbol{a}5(x, y)\}$ are column vectors of polynomial terms of the form $x^m y^n$.

Kinetic and Potential Energy of the Skins

To examine the procedures used to obtain stiffness and mass matrices due to contributions of different components of a typical built-up wing, a detailed derivation of the contributions of skin layers are presented next. The kinetic energy of an infinitesimal area $\mathrm{d}x\mathrm{d}y$ of a skin layer belonging to one of the wing box panels is

$$\mathrm{d}T = \tfrac{1}{2} \cdot \rho \cdot t(x, y) \cdot (\dot{u}^2 + \dot{v}^2 + \dot{w}^2) \cdot \mathrm{d}x \cdot \mathrm{d}y = \mathrm{d}T_u + \mathrm{d}T_v + \mathrm{d}T_w \tag{23}$$

where $\rho \cdot t(x, y)$ is the mass per unit area of the layer, and a dot over a time-dependent variable represents differentiation with respect to time. The velocities $\mathrm{d}u/\mathrm{d}t$, $\mathrm{d}v/\mathrm{d}t$, and $\mathrm{d}w/\mathrm{d}t$ can now be expressed in terms of the functions $u_0(x, y, t)$, $v_0(x, y, t)$, $w_0(x, y, t)$, $\phi_x(x, y, t)$, and $\phi_y(x, y, t)$, using Eqs. (3). For example, the $\mathrm{d}T_u$ term is calculated using

$$\mathrm{d}T_u = \tfrac{1}{2} \cdot \rho \cdot t(x, y) \cdot \dot{u}^2 \cdot \mathrm{d}x \cdot \mathrm{d}y \tag{24}$$

The velocity in the x direction is

$$\dot{u} = \frac{\mathrm{d}u}{\mathrm{d}t} = \frac{\mathrm{d}u_0}{\mathrm{d}t} - z \cdot \frac{\mathrm{d}(w_{0,x})}{\mathrm{d}t} + z \cdot \frac{\mathrm{d}\phi_x}{\mathrm{d}t} \tag{25}$$

$$\dot{u} = \{\boldsymbol{a}_1\}^T \cdot \{\dot{\boldsymbol{q}}1\} - z \cdot \{\boldsymbol{a}_{3,x}\}^T \cdot \{\dot{\boldsymbol{q}}3\} + z \cdot \{\boldsymbol{a}_4\}^T \cdot \{\dot{\boldsymbol{q}}4\} \tag{26}$$

Substitution of Eq. (26) into Eq. (24) leads to

$$\begin{aligned}\mathrm{d}T_u = \tfrac{1}{2} \cdot \rho \cdot t(x, y) \cdot \Big[&\{\dot{\boldsymbol{q}}1\}^T \cdot \{\boldsymbol{a}_1\} - z \cdot \{\dot{\boldsymbol{q}}3\}^T \cdot \{\boldsymbol{a}_{3,x}\} \\ &+ z \cdot \{\dot{\boldsymbol{q}}4\}^T \cdot \{\boldsymbol{a}_4\}\Big] \cdot \Big[\{\boldsymbol{a}_1\}^T \cdot \{\dot{\boldsymbol{q}}1\} - z \cdot \{\boldsymbol{a}_{3,x}\}^T \cdot \{\dot{\boldsymbol{q}}3\} \\ &+ z \cdot \{\boldsymbol{a}_4\}^T \cdot \{\dot{\boldsymbol{q}}4\}\Big] \cdot \mathrm{d}x \cdot \mathrm{d}y\end{aligned} \tag{27}$$

The vector multiplications are carried out, followed by x–y integration over the trapezoidal planform, leading to

$$\begin{aligned}T_u = &\frac{1}{2} \cdot \{\dot{\boldsymbol{q}}1\}^T \cdot \left[\int_x \int_y \rho \cdot t(x, y) \cdot \{\boldsymbol{a}_1\} \cdot \{\boldsymbol{a}_1\}^T \cdot \mathrm{d}x \cdot \mathrm{d}y\right] \cdot \{\dot{\boldsymbol{q}}1\} \\ &+ \frac{1}{2} \cdot \{\dot{\boldsymbol{q}}3\}^T \cdot \left[\int_x \int_y \rho \cdot t(x, y) \cdot z^2 \cdot \{\boldsymbol{a}_{3,x}\} \cdot \{\boldsymbol{a}_{3,x}\}^T \cdot \mathrm{d}x \cdot \mathrm{d}y\right] \cdot \{\dot{\boldsymbol{q}}3\} \\ &+ \frac{1}{2} \cdot \{\dot{\boldsymbol{q}}4\}^T \cdot \left[\int_x \int_y \rho \cdot t(x, y) \cdot z^2 \cdot \{\boldsymbol{a}_4\} \cdot \{\boldsymbol{a}_4\}^T \cdot \mathrm{d}x \cdot \mathrm{d}y\right] \cdot \{\dot{\boldsymbol{q}}4\} \\ &- \frac{1}{2} \cdot \{\dot{\boldsymbol{q}}1\}^T \cdot \left[\int_x \int_y \rho \cdot t(x, y) \cdot z \cdot \{\boldsymbol{a}_1\} \cdot \{\boldsymbol{a}_{3,x}\}^T \cdot \mathrm{d}x \cdot \mathrm{d}y\right] \cdot \{\dot{\boldsymbol{q}}3\} \\ &- \frac{1}{2} \cdot \{\dot{\boldsymbol{q}}3\}^T \cdot \left[\int_x \int_y \rho \cdot t(x, y) \cdot z \cdot \{\boldsymbol{a}_{3,x}\} \cdot \{\boldsymbol{a}_1\}^T \cdot \mathrm{d}x \cdot \mathrm{d}y\right] \cdot \{\dot{\boldsymbol{q}}1\} \\ &+ \frac{1}{2} \cdot \{\dot{\boldsymbol{q}}1\}^T \cdot \left[\int_x \int_y \rho \cdot t(x, y) \cdot z \cdot \{\boldsymbol{a}_1\} \cdot \{\boldsymbol{a}_4\}^T \cdot \mathrm{d}x \cdot \mathrm{d}y\right] \cdot \{\dot{\boldsymbol{q}}4\} \\ &+ \frac{1}{2} \cdot \{\dot{\boldsymbol{q}}4\}^T \cdot \left[\int_x \int_y \rho \cdot t(x, y) \cdot z \cdot \{\boldsymbol{a}_4\} \cdot \{\boldsymbol{a}_1\}^T \cdot \mathrm{d}x \cdot \mathrm{d}y\right] \cdot \{\dot{\boldsymbol{q}}1\} \\ &- \frac{1}{2} \cdot \{\dot{\boldsymbol{q}}3\}^T \cdot \left[\int_x \int_y \rho \cdot t(x, y) \cdot z^2 \cdot \{\boldsymbol{a}_{3,x}\} \cdot \{\boldsymbol{a}_4\}^T \cdot \mathrm{d}x \cdot \mathrm{d}y\right] \cdot \{\dot{\boldsymbol{q}}4\} \\ &- \frac{1}{2} \cdot \{\dot{\boldsymbol{q}}4\}^T \cdot \left[\int_x \int_y \rho \cdot t(x, y) \cdot z^2 \cdot \{\boldsymbol{a}_4\} \cdot \{\boldsymbol{a}_{3,x}\}^T \cdot \mathrm{d}x \cdot \mathrm{d}y\right] \cdot \{\dot{\boldsymbol{q}}3\}\end{aligned} \tag{28}$$

This expression can be rewritten as

$$T_u = \frac{1}{2} \cdot [\{\dot{\boldsymbol{q}}1\}^T \quad \{\dot{\boldsymbol{q}}3\}^T \quad \{\dot{\boldsymbol{q}}4\}^T] \cdot \begin{bmatrix} M^u_{11} & M^u_{13} & M^u_{14} \\ M^u_{31} & M^u_{33} & M^u_{34} \\ M^u_{41} & M^u_{43} & M^u_{44} \end{bmatrix} \cdot \begin{bmatrix} \{\dot{\boldsymbol{q}}1\} \\ \{\dot{\boldsymbol{q}}3\} \\ \{\dot{\boldsymbol{q}}4\} \end{bmatrix} \tag{29}$$

where the $[M_{ij}]$ represents mass submatrices. For example,

$$\begin{aligned}\left[M^u_{11}\right] = \int_x \int_y \rho \cdot \left(\sum_{k=1}^{Ntt} T(k) \cdot x^{mt(k)} \cdot y^{nt(k)}\right) \cdot \{\boldsymbol{a}_1(x, y)\} \\ \times \{\boldsymbol{a}_1(x, y)\}^T \cdot \mathrm{d}x \cdot \mathrm{d}y\end{aligned} \tag{30}$$

The matrix $[M^u_{11}]$ has dimension $N_{tu} \times N_{tu}$. Element (i, j) of this matrix is given by

$$\begin{aligned}\left[M^u_{11}\right](i, j) = \rho \sum_{k=1}^{Ntt} \Bigg(&T(k) \\ &\times \int_x \int_y \left(x^{mt(k)+mu(i)+mu(j)} y^{nt(k)+nu(i)+nu(j)} \cdot \mathrm{d}x \cdot \mathrm{d}y\right)\Bigg)\end{aligned} \tag{31}$$

or, using a more compact notation,

$$\left[M^u_{11}\right](i, j) = \rho \cdot \sum_{k=1}^{Ntt} (T(k) \cdot I_{\mathrm{TR}}(r, s)) \tag{32}$$

where

$$\begin{aligned}r &= mt(k) + mu(i) + mu(j) \\ s &= nt(k) + nu(i) + nu(j)\end{aligned} \tag{33}$$

$$I_{\mathrm{TR}}(r, s) = \int_x \int_y x^r y^s \, \mathrm{d}x \, \mathrm{d}y \tag{34}$$

is an area integral (over the trapezoidal that defines the planform). The value of this integral for any trapezoidal area can be found analytically without the need for any numerical integration.[10,12] A table of these integrals for all powers r, s required for the analysis of a wing segment has to be prepared only once at the beginning of the analysis. The element of the mass and stiffness matrices can be obtained using members of this table of integrals. Thus, no numerical integration is required in the present formulation.

The submatrix $[M^u_{33}]$ (dimension $N_{tw} \times N_{tw}$) is given by

$$\left[M^u_{33}\right] = \rho \cdot \int_x \int_y t(x, y) \cdot h^2(x, y) \cdot \{\boldsymbol{a}_{3,x}\} \cdot \{\boldsymbol{a}_{3,x}\}^T \cdot \mathrm{d}x \cdot \mathrm{d}y$$

$$= \rho \cdot \int_x \int_y \left(\sum_{k=1}^{Ntt} T(k) \cdot x^{mt(k)} \cdot y^{nt(k)} \right)$$

$$\times \left(\sum_{g=1}^{Nth} H(g) \cdot x^{mh(g)} \cdot y^{nh(g)} \right)$$

$$\times \left(\sum_{gg=1}^{Nth} H(gg) \cdot x^{mh(gg)} \cdot y^{nh(gg)} \right) \cdot \{\boldsymbol{a}_{3,x}\} \cdot \{\boldsymbol{a}_{3,x}\}^T \cdot \mathrm{d}x \cdot \mathrm{d}y \tag{35}$$

A typical element (i, j) of the mass submatrix $[M^u_{33}]$ is

$$\left[M^u_{33}\right](i, j) = \rho \cdot m_w(i) \cdot m_w(j) \cdot \sum_{k=1}^{Ntt} \sum_{g=1}^{Nth} \sum_{gg=1}^{Nth} T(k) \cdot H(g)$$

$$\times H(gg) \cdot I_{\mathrm{TR}}(r, s) \tag{36}$$

where

$$r = mt(k) + mh(g) + mh(gg) + [mw(i) - 1] + [mw(j) - 1]$$

$$s = nt(k) + nh(g) + nh(gg) + nw(i) + nw(j) \tag{37}$$

The double summation due to the presence of the h^2 term can result in heavy computational cost if many terms are needed in the $h(x, y)$ series. In an alternative approach, integral tables can be prepared for $t(x, y)$, $h(x, y)t(x, y)$, and $h^2(x, y)t(x, y)$ separately, and then used in the equations for mass and stiffness terms. Other mass submatrices can be calculated following the procedures described earlier. Using the expressions for $v(x, y, t)$ and $w(x, y, t)$, the kinetic energy contribution T_v can be expressed in matrix form as

$$T_v = \frac{1}{2} \cdot [\{\dot{\boldsymbol{q}}2\}^T \quad \{\dot{\boldsymbol{q}}3\}^T \quad \{\dot{\boldsymbol{q}}5\}^T] \cdot \begin{bmatrix} M^v_{22} & M^v_{23} & M^v_{25} \\ M^v_{32} & M^v_{33} & M^v_{35} \\ M^v_{52} & M^v_{53} & M^v_{55} \end{bmatrix} \cdot \begin{bmatrix} \{\dot{\boldsymbol{q}}2\} \\ \{\dot{\boldsymbol{q}}3\} \\ \{\dot{\boldsymbol{q}}5\} \end{bmatrix} \tag{38}$$

and because $\dot{w} = \{\boldsymbol{a}_3\}^T \cdot \{\dot{\boldsymbol{q}}3\}$, T_w can be expressed as

$$T_w = \tfrac{1}{2} \cdot \{\dot{\boldsymbol{q}}3\}^T \cdot \left[M^w_{33}\right] \cdot \{\dot{\boldsymbol{q}}3\} \tag{39}$$

where $[M^w_{33}]$ is given by

$$\left[M^w_{33}\right] = \int_x \int_y \rho \cdot t(x, y) \cdot \{\boldsymbol{a}_3\} \cdot \{\boldsymbol{a}_3\}^T \cdot \mathrm{d}x \cdot \mathrm{d}y \tag{40}$$

(dimension $N_{tw} \times N_{tw}$). Thus,

$$\left[M^w_{33}\right](i, j) = \rho \cdot \sum_{k=1}^{Ntt} T(k) \cdot I_{\mathrm{TR}}(r, s) \tag{41}$$

where

$$r = mt(k) + mw(i) + mw(j)$$

$$s = nt(k) + nw(i) + nw(j) \tag{42}$$

The total kinetic energy of the skin layer is finally computed by adding up the three different components:

$$T = T_u + T_v + T_w = \tfrac{1}{2} \cdot \{\dot{\boldsymbol{q}}\}^T \cdot [M] \cdot \{\dot{\boldsymbol{q}}\} \tag{43}$$

where

$$\{\dot{\boldsymbol{q}}\}^T = [\{\dot{\boldsymbol{q}}1\}^T \quad \{\dot{\boldsymbol{q}}2\}^T \quad \{\dot{\boldsymbol{q}}3\}^T \quad \{\dot{\boldsymbol{q}}4\}^T \quad \{\dot{\boldsymbol{q}}5\}^T] \tag{44}$$

and $[M]$ is the complete mass matrix for the skin layer. Its dimension is $N_{q\,\mathrm{tot}} \times N_{q\,\mathrm{tot}}$, where $N_{q\,\mathrm{tot}} = N_{tu} + N_{tv} + N_{tw} + N_{t\phi x} + N_{t\phi y}$. The matrix $[M]$ is given, on the basis of the rest of the mass submatrices defined earlier, by

$$[M] = \begin{bmatrix} M^u_{11} & 0 & M^u_{13} & M^u_{14} & 0 \\ 0 & M^v_{22} & M^v_{23} & 0 & M^v_{25} \\ M^u_{31} & M^v_{32} & M^{u+v+w}_{33} & M^u_{34} & M^v_{35} \\ M^u_{41} & 0 & M^u_{43} & M^u_{44} & 0 \\ 0 & M^u_{52} & M^v_{53} & 0 & M^v_{55} \end{bmatrix} \tag{45}$$

To find the mass matrix due to the group of N skin layers, mass matrices must be added layer by layer:

$$[M]_{\mathrm{total}} = [M]_{\mathrm{layer1}} + [M]_{\mathrm{layer2}} + \cdots + [M]_{\mathrm{layer}N} \tag{46}$$

or, alternatively, all layer thicknesses are added up to form a single-thickness polynomial [Eq. (10)] for the whole skin segment, and the mass matrix is evaluated for this total thickness.

For an individual composite skin layer, the contribution to the potential or strain energy U of an infinitesimally small skin element of surface area $\mathrm{d}x\,\mathrm{d}y$ is[10,13]

$$\mathrm{d}U = \frac{1}{2} \cdot t(x, y) \cdot [\varepsilon_{xx} \quad \varepsilon_{yy} \quad \gamma_{xy}] \cdot \begin{bmatrix} \sigma_{xx} \\ \sigma_{yy} \\ \sigma_{xy} \end{bmatrix} \cdot \mathrm{d}x \cdot \mathrm{d}y$$

$$= \frac{1}{2} \cdot t(x, y) \cdot [\varepsilon_{xx} \quad \varepsilon_{yy} \quad \gamma_{xy}] \cdot [Q] \cdot \begin{bmatrix} \varepsilon_{xx} \\ \varepsilon_{yy} \\ \gamma_{xy} \end{bmatrix} \cdot \mathrm{d}x \cdot \mathrm{d}y \tag{47}$$

where the constitutive matrix for the layer (depending on material properties and fiber direction) is $[Q]$.

The strains can be expressed in terms of all generalized displacements and rotations $\{\boldsymbol{q}1\}$ to $\{\boldsymbol{q}5\}$ in matrix form as follows:

$$\begin{bmatrix} \varepsilon_{xx} \\ \varepsilon_{yy} \\ \gamma_{xy} \end{bmatrix} = \begin{bmatrix} E_{11} & 0 & E_{13} & E_{14} & 0 \\ 0 & E_{22} & E_{23} & 0 & E_{25} \\ E_{31} & E_{32} & E_{33} & E_{34} & E_{35} \end{bmatrix} \cdot \begin{bmatrix} \{\boldsymbol{q}1\} \\ \{\boldsymbol{q}2\} \\ \{\boldsymbol{q}3\} \\ \{\boldsymbol{q}4\} \\ \{\boldsymbol{q}5\} \end{bmatrix}$$

$$+ \frac{1}{2} \begin{bmatrix} \{\boldsymbol{q}3\}^T & 0 & 0 \\ 0 & \{\boldsymbol{q}3\}^T & 0 \\ 0 & 0 & \{\boldsymbol{q}3\}^T \end{bmatrix} \cdot \begin{bmatrix} E_{16} \\ E_{26} \\ E_{36} \end{bmatrix} \cdot \{\boldsymbol{q}3\} \tag{48}$$

where the matrices $[E_{ij}]$ are matrices containing polynomial terms in x and y, defined (together with their dimensions) in the Appendix. The main product $[Q]\{\varepsilon\}$ can now be formed:

$$[Q] \cdot \{\varepsilon\} = \begin{bmatrix} A_{11} & A_{12} & A_{13} & A_{14} & A_{15} \\ A_{21} & A_{22} & A_{23} & A_{24} & A_{25} \\ A_{31} & A_{32} & A_{33} & A_{34} & A_{35} \end{bmatrix} \cdot \begin{bmatrix} \{\boldsymbol{q}1\} \\ \{\boldsymbol{q}2\} \\ \{\boldsymbol{q}3\} \\ \{\boldsymbol{q}4\} \\ \{\boldsymbol{q}5\} \end{bmatrix}$$

$$+ \frac{1}{2} \cdot \begin{bmatrix} Q_{11} \cdot \{\boldsymbol{q}3\}^T & Q_{12} \cdot \{\boldsymbol{q}3\}^T & Q_{16} \cdot \{\boldsymbol{q}3\}^T \\ Q_{21} \cdot \{\boldsymbol{q}3\}^T & Q_{22} \cdot \{\boldsymbol{q}3\}^T & Q_{26} \cdot \{\boldsymbol{q}3\}^T \\ Q_{61} \cdot \{\boldsymbol{q}3\}^T & Q_{62} \cdot \{\boldsymbol{q}3\}^T & Q_{66} \cdot \{\boldsymbol{q}3\}^T \end{bmatrix}$$

$$\times \begin{bmatrix} E_{16} \\ E_{26} \\ E_{36} \end{bmatrix} \cdot \{\boldsymbol{q}3\} \tag{49}$$

where the $[A_{ij}]$ submatrices have analogous dimensions to the $[E_{ij}]$, and are also given in the Appendix.

The product $[Q]\{\varepsilon\}$ [Eq. (49)] and the vector $\{\varepsilon\}^T$ [Eq. (48)] are substituted back into the definition of the potential energy [Eq. (47)], and integrated over the planform of the wing to yield

$$U = U_1 + U_2 + U_3 + U_4 = \tfrac{1}{2}\{\boldsymbol{q}\}^T[\boldsymbol{K}(\{\boldsymbol{q}\})]\{\boldsymbol{q}\} \tag{50}$$

where the first term U_1 is quadratic in $\{\boldsymbol{q}\}$; the second and the third terms U_2 and U_3 are cubic; and the fourth term U_4 is fourth order in $\{\boldsymbol{q}\}$. The terms are calculated one by one as follows:

$$U_1 = \frac{1}{2}\cdot\{\boldsymbol{q}\}^T \times \left(\int_x\int_y t(x,y)\cdot \begin{bmatrix} E_{11}^T & 0 & E_{31}^T \\ 0 & E_{22}^T & E_{32}^T \\ E_{13}^T & E_{23}^T & E_{33}^T \\ E_{14}^T & 0 & E_{34}^T \\ 0 & E_{25}^T & E_{35}^T \end{bmatrix} \cdot [A]\cdot \mathrm{d}x\cdot \mathrm{d}y \right) \cdot \{\boldsymbol{q}\} \tag{51}$$

or, using more compact notation,

$$U_1 = \tfrac{1}{2}\cdot\{\boldsymbol{q}\}^T\cdot[K_{\mathrm{LINEAR}}]\cdot\{\boldsymbol{q}\} \tag{52}$$

The matrix $[K_{\mathrm{LINEAR}}]$ is the linear part of the total $[K]$ matrix corresponding to a composite skin layer. It is constant and does not depend on $\{\boldsymbol{q}\}$. After carrying out the matrix multiplication and integration indicated in Eq. (51),

$$[K_{\mathrm{LINEAR}}] = \int_x\int_y \begin{bmatrix} B_{11} & B_{12} & B_{13} & B_{14} & B_{15} \\ B_{21} & B_{22} & B_{23} & B_{24} & B_{25} \\ B_{31} & B_{32} & B_{33} & B_{34} & B_{35} \\ B_{41} & B_{42} & B_{43} & B_{44} & B_{45} \\ B_{51} & B_{52} & B_{53} & B_{54} & B_{55} \end{bmatrix} \cdot t(x,y)\cdot \mathrm{d}x\cdot \mathrm{d}y = \begin{bmatrix} K_{L11} & K_{L12} & K_{L13} & K_{L14} & K_{L15} \\ K_{L21} & K_{L22} & K_{L23} & K_{L24} & K_{L25} \\ K_{L31} & K_{L32} & K_{L33} & K_{L34} & K_{L35} \\ K_{L41} & K_{L42} & K_{L43} & K_{L44} & K_{L45} \\ K_{L51} & K_{L52} & K_{L53} & K_{L54} & K_{L55} \end{bmatrix} \tag{53}$$

where, e.g.,

$$[K_{L11}] = \int_x\int_y t(x,y)\cdot[B_{11}]\cdot \mathrm{d}x\cdot \mathrm{d}y \tag{54}$$

$$[B_{11}] = Q_{11}\cdot E_{11}^T\cdot E_{11} + Q_{16}\cdot E_{11}^T\cdot E_{31} + Q_{61}\cdot E_{31}^T\cdot E_{11} + Q_{66}\cdot E_{31}^T\cdot E_{31} \tag{55}$$

Thus, using $Q_{ij} = Q_{ji}$,

$$[K_{L11}] = \int_x\int_y t(x,y)\cdot\left(Q_{11}\cdot\{\boldsymbol{a}_{1,x}\}\cdot\{\boldsymbol{a}_{1,x}\}^T + Q_{16}\cdot\{\boldsymbol{a}_{1,x}\}\cdot\{\boldsymbol{a}_{1,y}\}^T\right)\cdot \mathrm{d}x\cdot \mathrm{d}y + \int_x\int_y t(x,y)\cdot\left(Q_{16}\cdot\{\boldsymbol{a}_{1,y}\}\cdot\{\boldsymbol{a}_{1,x}\}^T + Q_{66}\cdot\{\boldsymbol{a}_{1,y}\}\cdot\{\boldsymbol{a}_{1,y}\}^T\right)\cdot \mathrm{d}x\cdot \mathrm{d}y \tag{56}$$

The element (i, j) of the matrix $[K_{L11}]$ can then be written as

$$\begin{aligned}[K_{L11}](i,j) = {} & Q_{11}\cdot mu(i)\cdot mu(j)\cdot\sum_{k=1}^{Ntt} T(k)\cdot I_{\mathrm{TR}}(r1,s1) \\ & + Q_{16}\cdot nu(i)\cdot mu(j)\cdot\sum_{k=1}^{Ntt} T(k)\cdot I_{\mathrm{TR}}(r2,s2) \\ & + Q_{16}\cdot mu(i)\cdot nu(j)\cdot\sum_{k=1}^{Ntt} T(k)\cdot I_{\mathrm{TR}}(r3,s3) \\ & + Q_{66}\cdot nu(i)\cdot nu(j)\cdot\sum_{k=1}^{Ntt} T(k)\cdot I_{\mathrm{TR}}(r4,s4)\end{aligned} \tag{57}$$

where the ri and si, the powers of polynomial terms, are given by

$$\begin{aligned} r1 &= mt(k) + [mu(i)-1] + [mu(j)-1] \\ s1 &= nt(k) + nu(i) + nu(j) \\ r2 &= mt(k) + mu(i) + [mu(j)-1] \\ s2 &= nt(k) + [nu(i)-1] + nu(j) \\ r3 &= mt(k) + [mu(i)-1] + mu(j) \\ s3 &= nt(k) + nu(i) + [nu(j)-1] \\ r4 &= mt(k) + mu(i) + mu(j) \\ s4 &= nt(k) + [nu(i)-1] + [nu(j)-1] \end{aligned} \tag{58}$$

The remaining linear $[K]$ matrix submatrices are derived in a similar way and can all be expressed by linear combinations of integral terms from the table of area integrals $I_{\mathrm{TR}}(m, n)$. The sum of the second and third elastic energy terms is given by

$$\begin{aligned} U_2 + U_3 = {} & \frac{1}{2}\cdot\int_x\int_y t(x,y)\frac{\{\boldsymbol{q}\}^T}{2}\begin{bmatrix} E_{11}^T & 0 & E_{31}^T \\ 0 & E_{22}^T & E_{32}^T \\ E_{13}^T & E_{23}^T & E_{33}^T \\ E_{14}^T & 0 & E_{34}^T \\ 0 & E_{25}^T & E_{35}^T \end{bmatrix} \\ & \times \begin{bmatrix} Q_{11}\cdot\{\boldsymbol{q}3\}^T & Q_{12}\cdot\{\boldsymbol{q}3\}^T & Q_{16}\cdot\{\boldsymbol{q}3\}^T \\ Q_{21}\cdot\{\boldsymbol{q}3\}^T & Q_{22}\cdot\{\boldsymbol{q}3\}^T & Q_{26}\cdot\{\boldsymbol{q}3\}^T \\ Q_{61}\cdot\{\boldsymbol{q}3\}^T & Q_{62}\cdot\{\boldsymbol{q}3\}^T & Q_{66}\cdot\{\boldsymbol{q}3\}^T \end{bmatrix}\cdot\begin{bmatrix} E_{16} \\ E_{26} \\ E_{36} \end{bmatrix} \\ & \times\{\boldsymbol{q}3\}\cdot\mathrm{d}x\cdot\mathrm{d}y + \frac{1}{2}\cdot\int_x\int_y t(x,y)\frac{\{\boldsymbol{q}3\}^T}{2}\cdot\begin{bmatrix} E_{16}^T & E_{26}^T & E_{36}^T \end{bmatrix} \\ & \times\begin{bmatrix} \{\boldsymbol{q}3\} & 0 & 0 \\ 0 & \{\boldsymbol{q}3\} & 0 \\ 0 & 0 & \{\boldsymbol{q}3\} \end{bmatrix}[A]\cdot\{\boldsymbol{q}\}\cdot\mathrm{d}x\cdot\mathrm{d}y \end{aligned} \tag{59}$$

Because the resultant matrices inside the first and second integrals are the transpose of each other, the previous equation can be written as

$$U_2 + U_3 = \frac{1}{2}\{\boldsymbol{q}\}^T\int_x\int_y\frac{t(x,y)}{2} \times \begin{bmatrix} 0 & 0 & C1^T & 0 & 0 \\ 0 & 0 & C2^T & 0 & 0 \\ C1 & C2 & C3+C3^T & C4 & C5 \\ 0 & 0 & C4^T & 0 & 0 \\ 0 & 0 & C5^T & 0 & 0 \end{bmatrix}\cdot\mathrm{d}x\cdot\mathrm{d}y\cdot\{\boldsymbol{q}\} \tag{60}$$

where the matrices $[C1]-[C5]$ contain terms that depend on $\{\boldsymbol{q}\}$ and are polynomial functions of x and y (see the Appendix).

The fourth contribution to the elastic energy of a skin layer is given by U_4:

$$U_4 = \frac{1}{2}\cdot\int_x\int_y t(x,y)\frac{\{\boldsymbol{q}3\}^T}{2}\cdot\begin{bmatrix}E_{16}^T & E_{26}^T & E_{36}^T\end{bmatrix}\times\begin{bmatrix}\{\boldsymbol{q}3\} & 0 & 0\\ 0 & \{\boldsymbol{q}3\} & 0\\ 0 & 0 & \{\boldsymbol{q}3\}\end{bmatrix}\times\begin{bmatrix}Q_{11}\cdot\{\boldsymbol{q}3\}^T & Q_{12}\cdot\{\boldsymbol{q}3\}^T & Q_{16}\cdot\{\boldsymbol{q}3\}^T\\ Q_{21}\cdot\{\boldsymbol{q}3\}^T & Q_{22}\cdot\{\boldsymbol{q}3\}^T & Q_{26}\cdot\{\boldsymbol{q}3\}^T\\ Q_{61}\cdot\{\boldsymbol{q}3\}^T & Q_{62}\cdot\{\boldsymbol{q}3\}^T & Q_{66}\cdot\{\boldsymbol{q}3\}^T\end{bmatrix}\cdot\begin{bmatrix}E_{16}\\ E_{26}\\ E_{36}\end{bmatrix}\times\{\boldsymbol{q}3\}\cdot\mathrm{d}x\cdot\mathrm{d}y \tag{61}$$

The result can be expressed more concisely by

$$U_4 = \frac{1}{2}\cdot\{\boldsymbol{q}3\}^T\cdot\left(\int_x\int_y\frac{t(x,y)}{4}\cdot[D]\cdot\mathrm{d}x\cdot\mathrm{d}y\right)\cdot\{\boldsymbol{q}3\} \tag{62}$$

where the matrix $[D]$ depends on polynomial terms in x and y and on $\{\boldsymbol{q}3\}\{\boldsymbol{q}3\}^T$, $[D]=[D(\{\boldsymbol{q}3\}\{\boldsymbol{q}3\}^T)]$ (see the Appendix). Equations (59–62) can now be added to yield

$$U_2+U_3+U_4 = \frac{1}{2}\{\boldsymbol{q}\}^T\int_x\int_y\frac{t(x,y)}{2}\times\begin{bmatrix}0 & 0 & C1^T & 0 & 0\\ 0 & 0 & C2^T & 0 & 0\\ C1 & C2 & C3+C3^T+\dfrac{D}{2} & C4 & C5\\ 0 & 0 & C4^T & 0 & 0\\ 0 & 0 & C5^T & 0 & 0\end{bmatrix}\times\mathrm{d}x\cdot\mathrm{d}y\cdot\{\boldsymbol{q}\} \tag{63}$$

An x, y integration over the planform area of the wing leads to

$$U_2+U_3+U_4 = \frac{1}{2}\{\boldsymbol{q}\}^T\times\begin{bmatrix}0 & 0 & K_{\mathrm{NL}13} & 0 & 0\\ 0 & 0 & K_{\mathrm{NL}23} & 0 & 0\\ K_{\mathrm{NL}31} & K_{\mathrm{NL}32} & K_{\mathrm{NL}33} & K_{\mathrm{NL}34} & K_{\mathrm{NL}35}\\ 0 & 0 & K_{\mathrm{NL}43} & 0 & 0\\ 0 & 0 & K_{\mathrm{NL}53} & 0 & 0\end{bmatrix}\cdot\{\boldsymbol{q}\} = \frac{1}{2}\{\boldsymbol{q}\}^T\cdot[K_{\mathrm{NL}}]\cdot\{\boldsymbol{q}\} \tag{64}$$

The next step is to define the submatrices $[N_{\mathrm{NL}ij}]$. The procedure is very similar to that used with the linear part of the $[K]$ matrix. Submatrices are first written based on their dependence on $[C_{ij}]$ and $[D]$ matrices. Then $[C_{ij}]$ and $[D]$ matrices are expressed as a function of the x, y-dependent $[E_{ij}]$ and the $\{\boldsymbol{q}3\}$ terms, so that finally $[K_{\mathrm{NL}ij}]$ can be found using summations of known terms selected from the table of area integrals, e.g.,

$$[K_{\mathrm{NL}13}] = \int_x\int_y\frac{t(x,y)}{2}\cdot[C1]^T\cdot\mathrm{d}x\cdot\mathrm{d}y \tag{65}$$

where, based on the expressions for the $[C]$ and $[E]$ matrices,

$$\begin{aligned}[K_{\mathrm{NL}13}] &= \int_x\int_y\frac{t(x,y)}{2}\cdot Q_{11}\cdot\{\boldsymbol{a}_{1,x}\}\cdot\{\boldsymbol{q}3\}^T\cdot\{\boldsymbol{a}_{3,x}\}\cdot\{\boldsymbol{a}_{3,x}\}^T\cdot\mathrm{d}x\cdot\mathrm{d}y\\ &+\int_x\int_y\frac{t(x,y)}{2}\cdot Q_{12}\cdot\{\boldsymbol{a}_{1,x}\}\cdot\{\boldsymbol{q}3\}^T\cdot\{\boldsymbol{a}_{3,y}\}\cdot\{\boldsymbol{a}_{3,y}\}^T\cdot\mathrm{d}x\cdot\mathrm{d}y\\ &+\int_x\int_y\frac{t(x,y)}{2}\cdot Q_{16}\cdot\{\boldsymbol{a}_{1,x}\}\cdot\{\boldsymbol{q}3\}^T\cdot 2\{\boldsymbol{a}_{3,x}\}\cdot\{\boldsymbol{a}_{3,y}\}^T\cdot\mathrm{d}x\cdot\mathrm{d}y\\ &+\int_x\int_y\frac{t(x,y)}{2}\cdot Q_{16}\cdot\{\boldsymbol{a}_{1,y}\}\cdot\{\boldsymbol{q}3\}^T\cdot\{\boldsymbol{a}_{3,x}\}\cdot\{\boldsymbol{a}_{3,x}\}^T\cdot\mathrm{d}x\cdot\mathrm{d}y\\ &+\int_x\int_y\frac{t(x,y)}{2}\cdot Q_{26}\cdot\{\boldsymbol{a}_{1,y}\}\cdot\{\boldsymbol{q}3\}^T\cdot\{\boldsymbol{a}_{3,y}\}\cdot\{\boldsymbol{a}_{3,y}\}^T\cdot\mathrm{d}x\cdot\mathrm{d}y\\ &+\int_x\int_y\frac{t(x,y)}{2}\cdot Q_{66}\cdot\{\boldsymbol{a}_{1,y}\}\cdot\{\boldsymbol{q}3\}^T\cdot 2\{\boldsymbol{a}_{3,x}\}\cdot\{\boldsymbol{a}_{3,y}\}^T\cdot\mathrm{d}x\cdot\mathrm{d}y\end{aligned} \tag{66}$$

It is now possible to identify contributions from individual polynomial terms $x^m y^n$ and use analytic integrations (and the integral table I_{TR}) to express

$$\begin{aligned}[K_{\mathrm{NL}13}](i,j) &= \frac{Q_{11}}{2}\cdot mu(i)\cdot mw(j)\times\sum_{k=1}^{Ntt}\sum_{l=1}^{N_{tw}}mw(l)\cdot T(k)\cdot q3(l)\cdot I_{\mathrm{TR}}(r1,s1)\\ &+\frac{Q_{12}}{2}\cdot mu(i)\cdot nw(j)\cdot\sum_{k=1}^{Ntt}\sum_{l=1}^{N_{tw}}nw(l)\cdot T(k)\cdot q3(l)\cdot I_{\mathrm{TR}}(r2,s2)\\ &+Q_{16}\cdot mu(i)\cdot nw(j)\cdot\sum_{k=1}^{Ntt}\sum_{l=1}^{N_{tw}}mw(l)\cdot T(k)\cdot q3(l)\cdot I_{\mathrm{TR}}(r3,s3)\\ &+\frac{Q_{16}}{2}\cdot nu(i)\cdot mw(j)\cdot\sum_{k=1}^{Ntt}\sum_{l=1}^{N_{tw}}mw(l)\cdot T(k)\cdot q3(l)\cdot I_{\mathrm{TR}}(r4,s4)\\ &+\frac{Q_{26}}{2}\cdot nu(i)\cdot nw(j)\cdot\sum_{k=1}^{Ntt}\sum_{l=1}^{N_{tw}}nw(l)\cdot T(k)\cdot q3(l)\cdot I_{\mathrm{TR}}(r5,s5)\\ &+Q_{66}\cdot nu(i)\cdot nw(j)\cdot\sum_{k=1}^{Ntt}\sum_{l=1}^{N_{tw}}mw(l)\cdot T(k)\cdot q3(l)\cdot I_{\mathrm{TR}}(r6,s6)\end{aligned} \tag{67}$$

where the resulting powers in each term are

$$\begin{aligned}r1 &= mt(k)+[mw(l)-1]+[mu(i)-1]+[mw(j)-1]\\ s1 &= nt(k)+nw(l)+nu(i)+nw(j)\\ r2 &= mt(k)+mw(l)+[mu(i)-1]+mw(j)\\ s2 &= nt(k)+[nw(l)-1]+nu(i)+[nw(j)-1]\\ r3 &= mt(k)+[mw(l)-1]+[mu(i)-1]+mw(j)\\ s3 &= nt(k)+nw(l)+nu(i)+[nw(j)-1]\\ r4 &= mt(k)+[mw(l)-1]+mu(i)+[mw(j)-1]\\ s4 &= nt(k)+nw(l)+[nu(i)-1]+nw(j)\\ r5 &= mt(k)+mw(l)+mu(i)+mw(j)\\ s5 &= nt(k)+[nw(l)-1]+[nu(i)-1]+[nw(j)-1]\\ r6 &= mt(k)+[mw(l)-1]+mu(i)+mw(j)\\ s6 &= nt(k)+nw(l)+[nu(i)-1]+[nw(j)-1]\end{aligned} \tag{68}$$

Other submatrices $[K_{\mathrm{NL}ij}]$ are obtained in a similar way. The derivation is tedious,[18] but straightforward. Symmetry of the $[K]$ matrix is used and there is no need to evaluate all submatrices. Matrices such as $[K_{\mathrm{NL}31}]$, $[K_{\mathrm{NL}32}]$, $[K_{\mathrm{NL}43}]$, and $[K_{\mathrm{NL}53}]$ can be simply found by calculating $[K_{\mathrm{NL}13}]^T$, $[K_{\mathrm{NL}23}]^T$, $[K_{\mathrm{NL}34}]^T$, and $[K_{\mathrm{NL}35}]^T$.

Note that the nonlinear part of the $[K]$ matrix $[K_{\mathrm{NL}ij}]$ depends on the $\{\boldsymbol{q}\}$ vector in two ways. The $\{\boldsymbol{q}\}$ dependent terms in the $[C_i]$ matrices lead to a linear dependence of the stiffness on $\{\boldsymbol{q}\}$. The $\{\boldsymbol{q}3\}$ dependent matrix $[D]$ leads to a quadratic dependence of the stiffness on $\{\boldsymbol{q}\}$. This quadratic dependence on $\{\boldsymbol{q}3\}$ appears in the submatrix $[K_{\mathrm{NL}33}]$ [Eqs. (63) and (64)]. The total elastic energy can now be assembled layer by layer, to yield the linear and nonlinear $[K]$ matrices. The nonlinear part, of course, depends on the deformation vector of generalized displacements $\{\boldsymbol{q}\}$:

$$U = U_1 + U_2 + U_3 + U_4 = \tfrac{1}{2} \cdot \{\boldsymbol{q}\}^T \cdot ([K_L] + [K_{\mathrm{NL}}(\{\boldsymbol{q}\})]) \cdot \{\boldsymbol{q}\} \tag{69}$$

Using techniques similar to those described earlier, mass and stiffness contributions of spar and rib webs can be obtained[18,20] for cases in which the spars and the ribs are modeled discretely and cases where spar and rib transverse shear contribution is smeared over the wing area. In any case, the wing box is modeled as a sandwich plate, and spar or web transverse shear contribution is integrated in the depth direction z from the bottom skin surface to the upper skin surface, and over the spar/rib lines (discrete spars/ribs) or over the area of the wing (smeared spars/ribs). As Refs. 18 and 20 show, the contribution of spar and rib webs to the total stiffness of the wing box, when the webs carry pure shear, affects only the linear part of the stiffness matrix; i.e., only the B_{44}, B_{45}, B_{54}, and B_{55} partitions of Eq. (53).

Equations of Motion

As already indicated, the unknown coefficients of the polynomial series used to approximate the functions $u_0(x, y)$, $v_0(x, y)$, $w_0(x, y)$, $\phi_x(x, y)$, and $\phi_y(x, y)$ [Eqs. (18–22)] are the generalized coordinates for the purpose of deriving Lagrange's equations. The expressions for kinetic energy T and potential energy U have already been given in terms of these generalized coordinates [Eqs. (43–45)]. Thus, there will be a total of $N_{q\,\mathrm{tot}}$ equations of motion corresponding to $N_{q\,\mathrm{tot}}$ $q(i)$ coefficients. It is straightforward to obtain the inertial component of the equations, because T is quadratic in $\{\dot{\boldsymbol{q}}\}$, $T = \frac{1}{2}\{\dot{\boldsymbol{q}}\}^T[M]\{\dot{\boldsymbol{q}}\}$, where the mass matrix is constant. For the contribution of geometrically nonlinear elastic forces, we need to differentiate the potential energy expression with respect to generalized deformations $\partial U/\partial q(j)$ as follows [Eq. (69)]:

$$\frac{\partial U}{\partial q(j)} = [0 \quad 0 \quad \cdots \quad 0 \quad 1 \quad 0 \quad \cdots \quad 0] \cdot [K] \cdot \{\boldsymbol{q}\} + \frac{1}{2} \cdot \{\boldsymbol{q}\}^T \cdot \left(\frac{\partial K_{\mathrm{NL}}}{\partial q(j)}\right) \cdot \{\boldsymbol{q}\} \tag{70}$$

Because the matrix $[K_{\mathrm{NL}}]$ depends only on $\{\boldsymbol{q}3\}$, and using the notation $\partial K_{\mathrm{NL}}/\partial q(j) = [K_{\mathrm{NL},q(j)}]$,

$$\frac{\partial K_{\mathrm{NL}}}{\partial q(j)} = \begin{bmatrix} 0 & 0 & K_{\mathrm{NL}13,q(j)} & 0 & 0 \\ 0 & 0 & K_{\mathrm{NL}23,q(j)} & 0 & 0 \\ K_{\mathrm{NL}31,q(j)} & K_{\mathrm{NL}32,q(j)} & K_{\mathrm{NL}33,q(j)} & K_{\mathrm{NL}34,q(j)} & K_{\mathrm{NL}35,q(j)} \\ 0 & 0 & K_{\mathrm{NL}43,q(j)} & 0 & 0 \\ 0 & 0 & K_{\mathrm{NL}53,q(j)} & 0 & 0 \end{bmatrix} \tag{71}$$

The expressions for different entries in $[K_{\mathrm{NL}}]$ are all available analytically and explicitly in terms of the $\{\boldsymbol{q}\}$ coordinates. Thus, evaluation of the matrix in Eq. (71) is straightforward. As an example, for the i, j element of the term $[K_{\mathrm{NL}13}]$ [Eqs. (66–68)], and focusing on the first few terms (the rest are differentiated in a similar way),

$$\frac{\partial K_{\mathrm{NL}13}}{\partial q(s)}(i, j) = \left[K_{\mathrm{NL}13,q(s)}\right](i, j) = \frac{Q_{11}}{2} mu(i) mw(j) \times \frac{\partial}{\partial q(s)} \left(\sum_{k=1}^{Ntt} \sum_{l=1}^{N_{tw}} mw(l) T(k) q3(l) I_{\mathrm{TR}}(r1, s1) \right) + \cdots \tag{72}$$

$$\left[K_{\mathrm{NL}13,q(s)}\right](i, j) = \frac{Q_{11}}{2} mu(i) mw(j) mw(s) \times \sum_{k=1}^{Ntt} T(k) \cdot I_{\mathrm{TR}}(r1, s1) + \cdots \tag{73}$$

where

$$r1 = mt(k) + [mw(s) - 1] + mu(i) + [mw(j) - 1]$$

$$s1 = nt(k) + nw(s) + nu(i) + nw(j) \tag{74}$$

where the index s is between $N_{tu} + N_{tv} + 1$ to $N_{tu} + N_{tv} + N_{tw}$; i.e., $q(s)$ is one of the elements of $\{\boldsymbol{q}3\}$. Other terms of $[K_{\mathrm{NL}13,q(s)}]$ and the matrices $[K_{\mathrm{NL}23,q(s)}]$, $[K_{\mathrm{NL}34,q(s)}]$, $[K_{\mathrm{NL}35,q(s)}]$, as well as the linear terms of $[K_{\mathrm{NL}33,q(s)}]$ are derived in this same way. Because $[K_{\mathrm{NL},q(s)}]$ is symmetric, matrices such as $[K_{\mathrm{NL}31,q(s)}]$ are immediately obtained using symmetry. As to terms of $[K_{\mathrm{NL}33,q(s)}]$ that correspond to the quadratic part of $[K_{\mathrm{NL}33}]$, their derivation is carried out using the explicit expressions [Eq. (64) and (65) and the Appendix]. For example, focusing on one of the terms shows

$$[K_{\mathrm{NL}33}](i, j) = \cdots + \frac{Q_{11}}{4} \cdot mw(i) \cdot mw(j) \cdot \sum_{k=1}^{Ntt} \sum_{l=1}^{N_{tw}} \sum_{ll=1}^{Nti} mw(l) \times mw(ll) \cdot T(k) \cdot q3(l) \cdot q3(ll) \cdot I_{\mathrm{TR}}(r25, s25) + \cdots \tag{75}$$

where

$$r25 = mt(k) + [mw(l) - 1] + [mw(ll) - 1] + [mw(i) - 1] + [mw(j) - 1]$$

$$s25 = nt(k) + nw(l) + nw(ll) + nw(i) + nw(j) \tag{76}$$

Then $[K_{\mathrm{NL}33,q(s)}](i, j)$ yields two terms as given by (s between $N_{tu} + N_{tv} + 1$ and $N_{tu} + N_{tv} + N_{tw}$):

$$\left[K_{\mathrm{NL}33,q(s)}\right](i, j) = \cdots + \frac{Q_{11}}{4} \cdot mw(i) \cdot mw(j) \cdot mw(s) \times \sum_{k=1}^{Ntt} \sum_{l=1}^{N_{tw}} mw(l) \cdot q3(l) \cdot I_{\mathrm{TR}}(r25ls, s25ls) + \frac{Q_{11}}{4} mw(i) \cdot mw(j) \cdot mw(s) \times \sum_{k=1}^{Ntt} \sum_{ll=1}^{N_{tw}} mw(ll) \cdot q3(ll) \cdot I_{\mathrm{TR}}(r25sll, s25sll) + \cdots \tag{77}$$

where

$$r25ls = mt(k) + [mw(l) - 1] + [mw(s) - 1] + [mw(i) - 1] + [mw(j) - 1]$$

$$s25ls = nt(k) + nw(l) + nw(s) + nw(i) + nw(j)$$

$$r25sll = mt(k) + [mw(s) - 1] + [mw(ll) - 1] + [mw(i) - 1] + [mw(j) - 1]$$

$$s25sll = nt(k) + nw(s) + nw(ll) + nw(i) + nw(j) \tag{78}$$

Finally,

$$\frac{\partial U}{\partial\{\boldsymbol{q}\}} = ([K_L] + [K_{\mathrm{NL}}] + [K_S]) \cdot \{\boldsymbol{q}\} = [K_f] \cdot \{\boldsymbol{q}\}$$

$$= \{\boldsymbol{R}_{\mathrm{elastic}}\} = \{\boldsymbol{R}_e\} \tag{79}$$

where the ith row of $[K_S]$ is $\frac{1}{2} \cdot \{\boldsymbol{q}\}^T \cdot [\partial K_{\mathrm{NL}}/\partial q(i)]$, and $\{\boldsymbol{R}_e\}$ is the vector of elastic forces.

Finally, the equations of motion of the entire system are represented by

$$[M] \cdot \{\ddot{\boldsymbol{q}}\} + [K_f] \cdot \{\boldsymbol{q}\} = [M] \cdot \{\ddot{\boldsymbol{q}}\} + \{\boldsymbol{R}_e\} = \{\boldsymbol{P}\} \tag{80}$$

where structural damping can be added directly[21] or via the generalized force vector $\{\boldsymbol{P}\}$.

External Forces

Distributed loads, with components in the x, y, and z directions, are expanded in terms of simple polynomial series:

$$P_x(x, y, t) = \sum_{i=1}^{Ntfrx} Fr_x(i) \cdot x^{mrfx(i)} \cdot y^{nrfx(i)} = \{\boldsymbol{a}_{frx}\}^T \cdot \{\boldsymbol{Fr}_x\}$$

$$P_y(x, y, t) = \sum_{i=1}^{Ntfry} Fr_y(i) \cdot x^{mrfy(i)} \cdot y^{nrfy(i)} = \{\boldsymbol{a}_{fry}\}^T \cdot \{\boldsymbol{Fr}_y\}$$

$$P_z(x, y, t) = \sum_{i=1}^{Ntfrz} Fr_z(i) \cdot x^{mrfz(i)} \cdot y^{nrfz(i)} = \{\boldsymbol{a}_{frz}\}^T \cdot \{\boldsymbol{Fr}_z\} \tag{81}$$

The coefficients $\{\boldsymbol{Fr}\}$ can be either constant or time dependent. They can be independent of or dependent on the motion itself via dependence on the generalized deformations $\{\boldsymbol{q}\}$. Following Ref. 13, the virtual work done by the distributed loads acting on a layer at distance z from $z = 0$ is $\delta Q = \delta Q_x + \delta Q_y + \delta Q_z$, where

$$\delta Q_x = P_x(x, y, t) \cdot \delta u(x, y, z, t) \cdot \mathrm{d}x \cdot \mathrm{d}y$$

$$\delta Q_y = P_y(x, y, t) \cdot \delta v(x, y, z, t) \cdot \mathrm{d}x \cdot \mathrm{d}y$$

$$\delta Q_z = P_z(x, y, t) \cdot \delta w(x, y, z, t) \cdot \mathrm{d}x \cdot \mathrm{d}y \tag{82}$$

and by using Eqs. (3) we obtain

$$\delta Q_x = P_x \cdot (\delta u_0 - z \cdot \delta w_{0,x} + z \cdot \delta\phi_x) \cdot \mathrm{d}x \cdot \mathrm{d}y$$

$$\delta Q_y = P_y \cdot (\delta v_0 - z \cdot \delta w_{0,y} + z \cdot \delta\phi_y) \cdot \mathrm{d}x \cdot \mathrm{d}y$$

$$\delta Q_z = P_z \cdot \delta w_0 \cdot \mathrm{d}x \cdot \mathrm{d}y \tag{83}$$

Using the polynomial approximations to the displacement functions u_0, v_0, w_0, ϕ_x, and ϕ_y [Eqs. (18–22)], the total work done by the external forces on a layer at some z elevation is given by

$$\delta Q = \int_x \int_y \Big[P_x \cdot \{\boldsymbol{a}_1\}^T \cdot \{\delta\boldsymbol{q}1\} + P_y \cdot \{\boldsymbol{a}_2\}^T \cdot \{\delta\boldsymbol{q}2\}$$

$$+ \left(P_z \cdot \{\boldsymbol{a}_3\}^T - z \cdot P_x \cdot \{\boldsymbol{a}_{3,x}\}^T - z \cdot P_y \cdot \{\boldsymbol{a}_{3,y}\}^T \right) \cdot \{\delta\boldsymbol{q}3\}$$

$$+ z \cdot P_x \cdot \{\boldsymbol{a}_4\}^T \cdot \{\delta\boldsymbol{q}4\} + z \cdot P_y \cdot \{\boldsymbol{a}_5\}^T \cdot \{\delta\boldsymbol{q}5\} \Big] \cdot \mathrm{d}x \cdot \mathrm{d}y \tag{84}$$

from which the generalized load vector can be defined as

$$\{\boldsymbol{P}\}^T = \begin{bmatrix} \{\boldsymbol{P}1\}^T & \{\boldsymbol{P}2\}^T & \{\boldsymbol{P}3\}^T & \{\boldsymbol{P}4\}^T & \{\boldsymbol{P}5\}^T \end{bmatrix} \tag{85}$$

Notice that z establishes at what height the load is being applied. Each of the individual vectors that appear in Eq. (85) can be expressed as a linear combination of area integrals. For example, $\{\boldsymbol{P}1\}$ and $\{\boldsymbol{P}3\}$ are as follows:

$$\{\boldsymbol{P}1\} = \int_x \int_y P_x \cdot \{\boldsymbol{a}_1\} \cdot \mathrm{d}x \cdot \mathrm{d}y$$

$$= \int_x \int_y \{\boldsymbol{Fr}_x\}^T \cdot \{\boldsymbol{a}_{frx}\} \cdot \{\boldsymbol{a}_1\} \cdot \mathrm{d}x \cdot \mathrm{d}y$$

$$= \sum_{t=1}^{Nfrx} Fr_x(t) \cdot \int_x \int_y \{\boldsymbol{a}_1\} \cdot x^{mfrx(t)} \cdot y^{nfrx(t)} \cdot \mathrm{d}x \cdot \mathrm{d}y \tag{86}$$

The element (i) of the vector $\{\boldsymbol{P}1\}$ is then given by

$$\boldsymbol{P}1(i) = \sum_{t=1}^{Nfrx} Fr_x(t) \cdot I_{\mathrm{TR}}(r, s) \tag{87}$$

where

$$r = mfrx(t) + mu(i), \qquad s = nfrx(t) + nu(i) \tag{88}$$

Similarly,

$$\{\boldsymbol{P}3\} = \int_x \int_y (P_z \cdot \{\boldsymbol{a}_3\} - z \cdot P_x \cdot \{\boldsymbol{a}_{3,x}\} - z \cdot P_y \cdot \{\boldsymbol{a}_{3,y}\}) \cdot \mathrm{d}x \cdot \mathrm{d}y \tag{89}$$

and the ith element is

$$P3(i) = \sum_{t=1}^{Nfrz} Fr_z(t) \cdot I_{\mathrm{TR}}(r1, s1) - z \cdot mw(i) \cdot \sum_{t=1}^{Nfrx} Fr_x(t)$$

$$\times I_{\mathrm{TR}}(r2, s2) - z \cdot nw(i) \cdot \sum_{t=1}^{Nfry} Fr_y(t) \cdot I_{\mathrm{TR}}(r3, s3) \tag{90}$$

where

$$r1 = mfrz(t) + mw(i), \qquad s1 = nfrz(t) + nw(i)$$

$$r2 = mfrx(t) + [mw(i) - 1], \qquad s2 = nfrx(t) + nw(i)$$

$$r3 = mfry(t) + mw(i), \qquad s3 = nfry(t) + [nw(i) - 1] \tag{91}$$

If the concentrated loads are present, the previous derivation can be simplified. For a point load of value ($\hat{Fr}_x$, $\hat{Fr}_y$, and $\hat{Fr}_z$) applied at the point (x_a, y_a, and z_a) of the wing box, the generalized force vector $\{\boldsymbol{P}\}$ is given by

$$\{\boldsymbol{P}\} = \begin{bmatrix} \hat{Fr}_x \cdot \{\boldsymbol{a}_1\} \\ \hat{Fr}_y \cdot \{\boldsymbol{a}_2\} \\ \hat{Fr}_z \cdot \{\boldsymbol{a}_3\} - z_a \cdot \hat{Fr}_x \cdot \{\boldsymbol{a}_{3,x}\} - z_a \cdot \hat{Fr}_y \cdot \{\boldsymbol{a}_{3,y}\} \\ z_a \cdot \hat{Fr}_x \cdot \{\boldsymbol{a}_4\} \\ z_a \cdot \hat{Fr}_y \cdot \{\boldsymbol{a}_5\} \end{bmatrix} \tag{92}$$

where all of the polynomials $\{\boldsymbol{a}\}$ are evaluated at the point (x_a, y_a). Note again that both ($\hat{Fr}_x$, $\hat{Fr}_y$ and $\hat{Fr}_z$) for a point force or $\{\boldsymbol{Fr}_x\}$, $\{\boldsymbol{Fr}_y\}$, and $\{\boldsymbol{Fr}_z\}$ for distributed loads can be functions of the vector $\{\boldsymbol{q}\}$ (or, of the displacements u, v, and w, which are, in turn, functions of $\{\boldsymbol{q}\}$), thus representing deformation dependent loads.

Boundary Conditions

Zero-displacement boundary conditions can be imposed on the displacements (u, v, and w) in two ways. In the special case of

imposing cantilever boundary conditions along the lines $y=0$ or $x=0$, an appropriate choice of simple polynomials for the Ritz function series can reflect the presence of zero displacements. For example, in a cantilever case where (u, v, and w) are set equal to (0, 0, and 0) along $y=0$, the following choice of Ritz polynomials automatically satisfies the boundary conditions:

$$w(x,y)=\{\boldsymbol{y}^2,\boldsymbol{xy}^2,\boldsymbol{y}^3,\boldsymbol{xy},\boldsymbol{xy}^2,\boldsymbol{y}^3,\ldots,\ldots\}\begin{Bmatrix}\boldsymbol{q}3(1)\\ \boldsymbol{q}3(2)\\ \boldsymbol{q}3(3)\\ \cdots\\ \cdots\end{Bmatrix}$$

will guarantee $w=0$ and $w_{,y}=0$ along $y=0$.

Then the Ritz series

$$\{\boldsymbol{y},\boldsymbol{xy},\boldsymbol{y}^2,\boldsymbol{x}^2\boldsymbol{y},\boldsymbol{xy}^2,\boldsymbol{y}^3,\ldots,\ldots\}\begin{Bmatrix}\boldsymbol{ql}(1)\\ \boldsymbol{ql}(2)\\ \boldsymbol{ql}(3)\\ \cdots\\ \cdots\end{Bmatrix}$$

for $u_0(x,y)$, $v_0(x,y)$, $\phi_x(x,y)$, and $\phi_y(x,y)$ (the index l assuming values of 1, 2, 4, and 5, respectively) will complete the creation of admissible functions for this case.

A more general way to enforce boundary conditions is by using very stiff springs to limit deformation or to force a connection between two parts. If a point on the wing must be constrained so that its u, v, and w displacements be zero, then, introducing stiff springs with coefficients k_u, k_v, and k_w, the potential energy of the springs is

$$U_d=\tfrac{1}{2}\cdot k_u\cdot u^2+\tfrac{1}{2}\cdot k_v\cdot v^2+\tfrac{1}{2}\cdot k_w\cdot w^2 \tag{93}$$

For points at $z=0$, using the Ritz polynomial series [Eqs. (18–22)],

$$U_d=\frac{1}{2}\cdot\begin{bmatrix}\{\boldsymbol{q}1\}^T\\ \{\boldsymbol{q}2\}^T\\ \{\boldsymbol{q}3\}^T\end{bmatrix}^T\times\begin{bmatrix}k_u\{\boldsymbol{a}_1\}\{\boldsymbol{a}_1\}^T & 0 & 0\\ 0 & k_v\{\boldsymbol{a}_2\}\{\boldsymbol{a}_2\}^T & 0\\ 0 & 0 & k_w\{\boldsymbol{a}_3\}\{\boldsymbol{a}_3\}^T\end{bmatrix}\cdot\begin{bmatrix}\{\boldsymbol{q}1\}\\ \{\boldsymbol{q}2\}\\ \{\boldsymbol{q}3\}\end{bmatrix} \tag{94}$$

where the vectors of polynomials $\{\boldsymbol{a}_1\}$, $\{\boldsymbol{a}_2\}$, and $\{\boldsymbol{a}_3\}$ are evaluated at the spring coordinates (x_{sp}, y_{sp}). When plate rotations must be constrained, it is necessary to limit, via stiff rotational springs, the rotation in the x direction $\Psi_x=w_{,x}-\phi_x$, and the rotation in the y direction $\Psi_y=w_{,y}-\phi_y$. The potential energy associated with a rotational spring is

$$U_{rt}=\tfrac{1}{2}\cdot k_{rx}\cdot(w_{,x}-\phi_x)^2+\tfrac{1}{2}\cdot k_{ry}\cdot(w_{,y}-\phi_y)^2 \tag{95}$$

Note that if CPT is used these springs will impose zero $w_{,x}$ and $w_{,y}$ (ϕ_x and ϕ_y are identically zero). The terms in Eq. (95) are expressed using the polynomial expansion [Eqs. (18–22)]

$$U_{rt}=\left(\tfrac{1}{2}\cdot k_{rx}\cdot\left(w_{,x}^2-w_{,x}\cdot\phi_x-\phi_x\cdot w_{,x}+\phi_x^2\right)\right)+\left(\tfrac{1}{2}\cdot k_{ry}\cdot\left(w_{,y}^2-w_{,y}\cdot\phi_y-\phi_y\cdot w_{,y}+\phi_y^2\right)\right) \tag{96}$$

leading to

$$U_{rt}=\tfrac{1}{2}\cdot[\{\boldsymbol{q}3\}^T\quad\{\boldsymbol{q}4\}^T\quad\{\boldsymbol{q}5\}^T]\times\begin{bmatrix}[K33_{\mathrm{sp}}] & -k_{rx}\{\boldsymbol{a}_{3,x}\}\{\boldsymbol{a}_4\}^T & -k_{ry}\{\boldsymbol{a}_{3,y}\}\{\boldsymbol{a}_5\}^T\\ -k_{rx}\{\boldsymbol{a}_4\}\{\boldsymbol{a}_{3,x}\}^T & k_{rx}\{\boldsymbol{a}_4\}\{\boldsymbol{a}_4\}^T & 0\\ -k_{ry}\{\boldsymbol{a}_5\}\{\boldsymbol{a}_{3,y}\}^T & 0 & k_{ry}\{\boldsymbol{a}_5\}\{\boldsymbol{a}_5\}^T\end{bmatrix}\times\begin{bmatrix}\{\boldsymbol{q}3\}\\ \{\boldsymbol{q}4\}\\ \{\boldsymbol{q}5\}\end{bmatrix} \tag{97}$$

where

$$[K33_{\mathrm{sp}}]=k_{rx}\{\boldsymbol{a}_{3,x}\}\{\boldsymbol{a}_{3,x}\}^T+k_{ry}\{\boldsymbol{a}_{3,y}\}\{\boldsymbol{a}_{3,y}\}^T \tag{98}$$

Once again all of the vectors $\{\boldsymbol{a}\}$ are evaluated at (x_{sp}, y_{sp}), the coordinates of the rotational spring location. All stiff springs used to impose zero boundary conditions on points on the wing contribute to the linear part of the stiffness matrix $[K_L]$.

Experience with stiff springs for boundary-condition enforcement with the linear equivalent plate codes[7–14] shows that it is possible to find spring coefficient values that are stiff enough to impose the zero-deformation requirement, and at the same time are not too high a level that may lead to ill conditioning of the stiffness matrix. Actually, a quick convergence study, carried out by increasing the spring values by factors of 10 from about 5 orders of magnitude higher than typical real stiffness to about 10^{12} will usually be sufficient to select the values for analysis (double precision on a DEC Alpha work station).

Static Solution and Time-Integration Methods

The static equations can be separated into linear and nonlinear parts:

$$[K_f(\{\boldsymbol{q}\})]\cdot\{\boldsymbol{q}\}=([K_L]+[K_{\mathrm{NL}}(\{\boldsymbol{q}3\})]+[K_S(\{\boldsymbol{q}\})])\cdot\{\boldsymbol{q}\}=\{\boldsymbol{P}\} \tag{99}$$

and written in the form

$$\{\boldsymbol{f}\}=[K_f]\cdot\{\boldsymbol{q}\}-\{\boldsymbol{P}\}=\{\boldsymbol{0}\} \tag{100}$$

Expanding $\{\boldsymbol{f}\}$ in a Taylor series results in

$$\{\boldsymbol{f}\}(\{\boldsymbol{q}\}+\{\boldsymbol{\delta q}\})=\{\boldsymbol{f}\}(\{\boldsymbol{q}\})+\sum_{j=1}^{N_{q\,\mathrm{tot}}}\frac{\partial}{\partial q_j}\{\boldsymbol{f}\}\cdot\delta q_j+\mathcal{O}(\{\boldsymbol{\delta q}^2\}) \tag{101}$$

Linearizing and setting to zero, following a Newton–Raphson approach, leads to a linear system of equations:

$$[\alpha]\cdot\{\boldsymbol{\delta q}\}=-\{\boldsymbol{f}(\{\boldsymbol{q}\})\} \tag{102}$$

where

$$[\alpha](i,j)=\frac{\partial}{\partial q(j)}f(i)\bigg|_{\{\boldsymbol{q}\}} \tag{103}$$

$[\alpha]$, in this case, can be obtained in analytical form based on the explicit derivations described previously. Equation (100) is solved using a Newton–Raphson iteration imposed on an incremental approach, in which the loads are increased incrementally until they reach their final level.

For the dynamic case, a number of time-integration algorithms were included in the new nonlinear equivalent plate computer capability.[18] Simulation results shown here, however, were all obtained using the Newmark time-integration method. For information on this method and its applicability to nonlinear dynamic systems, the reader is referred to Refs. 21 and 22.

Test Problems

To assess the accuracy and computational performance of the new capability described in this paper, the polynomial-based equivalent plate technique was used to model a number of nonlinear beam and plate structures, for which other solutions were available. Results of systematic studies, in which the effect on the accuracy of Ritz polynomial orders was examined, can be found in Ref. 18. The presentation of results in this paper focuses on three test problems. The first and second involve solid plates, and the third problem involves a model wing box. Results of linear and nonlinear static analyses as well as dynamic response computations are discussed.

Full Plate

The present formulation, as developed earlier, is aimed at wing-box structures, made of thin cover skins held together by an array of spars and ribs. Stiffness and mass terms are, thus, derived for thin skins placed at $z = h_U(x, y)$ and $z = h_L(x, y)$, and for associated rib and spar webs connecting them. If full-core plates are to be modeled using the current polynomial Ritz approach, the formulations presented earlier must be slightly modified. This is done by changing the way in which each skin-layer contribution is integrated over the volume of the plate. All of the necessary modifications rely on replacing the skin-layer thickness T and height (z position) coefficients H [Eqs. (9) and (10)] by coefficients corresponding to upper and lower limits of the layer representing a full-core plate (between H_u and H_L), as follows:

$$\begin{aligned} &\text{Terms with} \quad T(k) \quad \text{are replaced by} \quad [H_u(g) - H_L(g)] \\ &\text{Terms with} \quad T^*H \quad \text{are replaced by} \quad \tfrac{1}{2}\left(H_u^2 - H_L^2\right) \\ &\text{Terms with} \quad T^*H^2 \quad \text{are replaced by} \quad \tfrac{1}{3}\left(H_u^3 - H_L^3\right) \end{aligned} \tag{104}$$

The strain energy of the skins must be further modified by including a new contribution of the type

$$U_{t\,\text{shear}} = \frac{1}{2}\iiint \begin{bmatrix} \gamma_{yz} \\ \gamma_{xz} \end{bmatrix}^T \cdot \begin{bmatrix} k_1^2 A_{44} & k_1 k_2 A_{45} \\ k_1 k_2 A_{45} & k_2^2 A_{55} \end{bmatrix} \cdot \begin{bmatrix} \gamma_{yz} \\ \gamma_{xz} \end{bmatrix} \cdot \mathrm{d}Vol \tag{105}$$

where k_1 and k_2 are correction factors accounting for the fact that the transverse shear stress is actually not constant across the section area.[23] If the solid full-core plate contains a number of composite layers, then the contribution of each layer to the mass and stiffness matrices is evaluated separately and then added up. Of course, rib and spar contributions are not taken into account when analyzing full-plate examples.

Square Simply Supported Isotropic Solid Plate

Results of nonlinear static analysis and experiments of this structure under uniform lateral pressure loading (with stress-free edges) are presented in Figs. 2.14 and 2.15 of Ref. 17. This is an extremely challenging problem for the capability developed in this work, because unlike typical wing-box structures for which the new capability is developed, here the plate is simply supported on all sides. Zero vertical displacement $w(x, y)$ boundary conditions must be imposed then along $x = 0$, $y = 0$, $x = a$, and $y = a$. This is done by choosing proper Ritz w polynomial terms, so that $w = 0$ along $x = 0$ and $y = 0$ is automatically satisfied. To impose $w = 0$ along $x = a$ and $y = a$, stiff vertical springs are distributed along these sides. Because the combination of stiff springs and high-order simple polynomials is known to lead to ill-conditioning with the simple polynomials used here, this becomes a challenging test of the limitations of the new method. Because of the freedom of edges to move in the x and y directions, all polynomial Ritz terms in the u and v expansions are used in the equivalent plate model. Only three soft springs are used to prevent rigid body motion in the x and y directions.

Short Cantilevered Plate

The short cantilevered plate is made from an isotropic material with $E = 90.0$ GPa, $v = 0.30$, and a density of 2700 kg/m^3. The plate was cantilevered and subject to a uniform vertical pressure over its area. Its chord was 30 cm long, and its length was set equal to 10 cm. Its thickness was 1 mm. Thus, no shear deformation was included in this case. Ten polynomial terms were used to expand each of the in-plane displacements u and v (y, xy, y^2, x^2y, xy^2, y^3, x^3y, x^2y^2, xy^3, and y^4). For the vertical displacement w, 15 terms were used (y^2, xy^2, y^3, x^2y^2, xy^3, y^4, x^3y^2, x^2y^3, xy^4, y^5, x^4y^2, x^3y^3, x^2y^4, xy^5, and y^6). Because cantilever boundary conditions are automatically satisfied by this choice of polynomial Ritz terms, no stiff springs were needed in the analysis.

The results from the nonlinear plate code developed here were compared with the results obtained with a nonlinear finite element model defined using the automatic dynamic incremental nonlinear analysis (ADINA).[24] Three hundred plate elements[24] were used to create the entire finite element model. Results of static and dynamic analyses were compared.

Wing Box

The wing-box test case is used to assess accuracy and performance of the new equivalent plate capability for wing-box structures, made of skins, spars, and ribs. The results obtained are compared to nonlinear finite element results obtained with ADINA.[24] The wing box presented here is 10 m long (with a 45-deg sweep), has a 2-m chord, and is 0.2 m deep. Only two spars (front and rear) are present. Ten ribs equally spaced along the wing are present as well. In addition to that, 10 spar caps (five on the upper surface, five on the lower surface) are included. Four of them correspond to the spar caps of the front and rear spars. The other six correspond to stiffeners (running in the direction of the spars), which are equally spaced along the width of the wing. Figure 2 shows a three-dimensional view of the finite element model. Part of the upper skin of the wing was removed in the figure to allow the view of the internal features of the model. An isotropic material was used for the entire structure. Its Young modulus was set equal to 68.95 GPa (with a 0.30 Poissons' ratio) and its density to 2709.7 kg/m^3. All of the skin thicknesses were set equal to 8.128×10^{-4} m and all of the spar- and rib-web thicknesses to 1.2954×10^{-3} m. The spar cap areas were set to be 2.3935×10^{-4} m^2 each and the stiffener areas to 3.9355×10^{-5} m^2.

Overall, 2 skins, 10 ribs, 2 spar webs, and 10 caps were included in the equivalent plate model of the wing box. The unknown functions ϕ_x and ϕ_y were included in the analysis to account for transverse shear. The wing is cantilevered at $y = 0$. Six Ritz terms were used to expand the in-plane displacements u and v (y, xy, y^2, x^2y, xy^2, and y^3). Fifteen Ritz terms were used for the vertical displacement w (y, xy, y^2, x^2y, xy^2, y^3, x^3y, x^2y^2, xy^3, y^4, x^4y, x^3y^2, x^2y^3, xy^4, and y^5), and 10 Ritz terms each were used for the shear deformations ϕ_x (y, xy, y^2, x^2y, xy^2, y^3, x^3y, x^2y^2, xy^3, and y^4) and ϕ_y (1, x, y, x^2, xy, y^2, x^3, x^2y, xy^2, and y^3). Stiff springs ($k = 1.0 \times 10^{12}$) were placed at the root of the wing box to enforce the zero rotation condition.

In the ADINA finite element model plate elements[24] were used for the skins and webs, and three-dimensional beam elements were used to represent the spar caps and stiffeners. Because shear web elements are not available in ADINA, an orthotropic material was used for the plate elements of the web, with $E_i = 1.0$ GPa, $G_{ij} = 26.52$ GPa, and $v_{ij} = 0$ to simulate shear web elements. To make up for the loss of stiffness in the vertical direction, 20 truss elements (10 on the front, 10 on the rear) were introduced connecting upper and lower skins. The chosen E for these elements was 68.95 GPa with a cross-sectional area of 1.2954×10^{-3} m^2. Overall, 560 plate elements, 100 three-dimensional beam elements, and 20 truss elements were used to define the nonlinear finite element model.

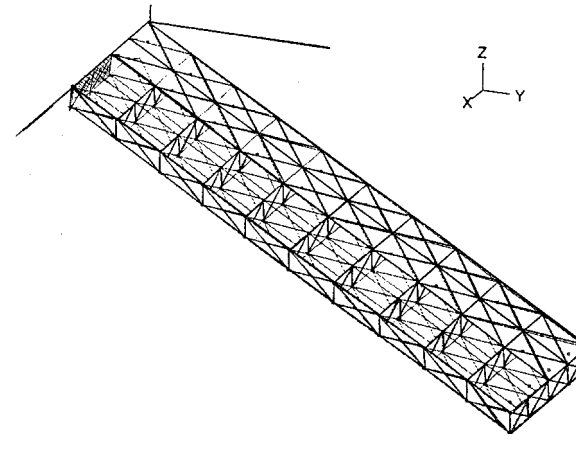

Fig. 2 Nonlinear finite element model of a three-dimensional wing box.

Solid Plate Results

Figures 3 and 4 compare results obtained with the current equivalent plate capability to results in Ref. 17. The Ritz expansions used consisted of 21 terms for u, 21 terms for v, and either 28 or 36 terms for w (both expansions led to results within 1% of one another). Note that there is no transverse shear modeled here and the analysis is therefore based on CPT.

As Figs. 3 and 4 show, the linear results are well matched and the nonlinear solution is very close to the computational and experimental results presented in Ref. 17.

Short Cantilevered Plate Results

Figure 5 shows normalized vertical tip deflection of the plate under static load. The nondimensional load parameter P_0a^4/Eh^4 (P_0 is the uniform pressure magnitude, a is the length, E is the Youngs modulus, and h is the thickness) was used to normalize the results. The vertical tip displacement of the plate was normalized by the plate length. The linear results from the plate code were about 3.5% stiffer than the linear results given by the ADINA model. For the nonlinear analysis the differences between the ADINA and the present work results were quite small as well. For load parameter values below 30.0 ($P_0 = 27.0$ kPa) the percent difference was smaller than 4%. For load parameter values between 30.0 and 45.0 ($P_0 = 40.5$ kPa) the percent difference ranged between 4 and 7%. The accuracy of the results obtained by the method developed here began to deteriorate with larger values. As long as the magnitude of the plate tip vertical deflection remained smaller than half the plate length, the results from both methods were very close.

It should be noted that the preceding calculations for the method developed here were repeated using a 21-polynomial term expansion for the w displacement. No meaningful differences with respect to the previously used 15-term expansion were observed. Simple stress calculations were performed for the previous case and the stresses were confirmed to be well under the yielding point.

Linear and nonlinear dynamic simulations are presented next. For a uniform pressure step load of 15.0 kPa (load parameter = 16.7) the time history of the normalized vertical tip displacement was calculated. See Fig. 6 for the linear case and Fig. 7 for the nonlinear case (same loading in both cases). The correlation between the results obtained with this program and with ADINA is good. For the linear case the period of the motion calculated using the present work was about 0.01039 s and the period obtained from the ADINA results was about 0.01045, a 0.7% difference. For the nonlinear case the period became smaller. This was expected because of the hardening effect observed in the nonlinear static analysis. The output from the code developed here shows a motion with a period of about

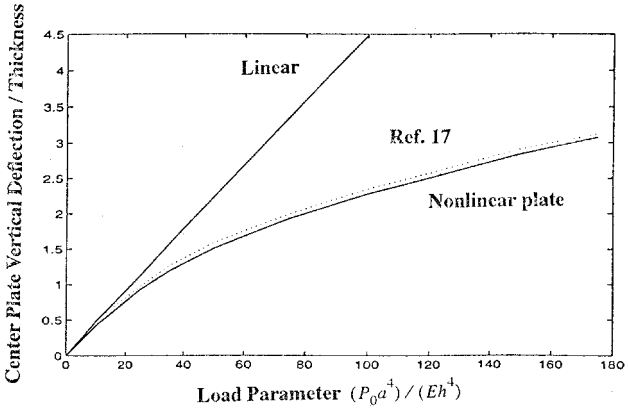

Fig. 3 Normalized center plate vertical deflection due to uniform pressure load, simply supported isotropic plate.

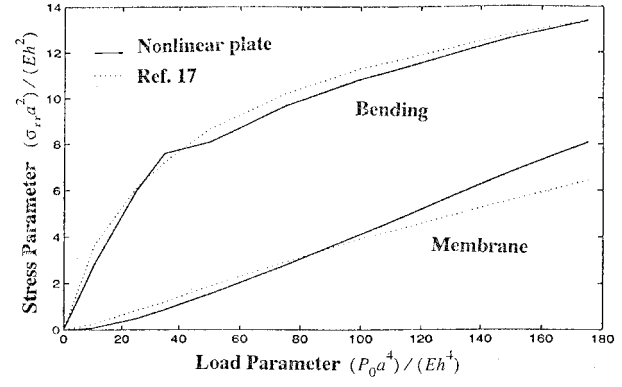

Fig. 4 Normalized center plate stress (x direction) due to uniform pressure load, simply supported isotropic plate.

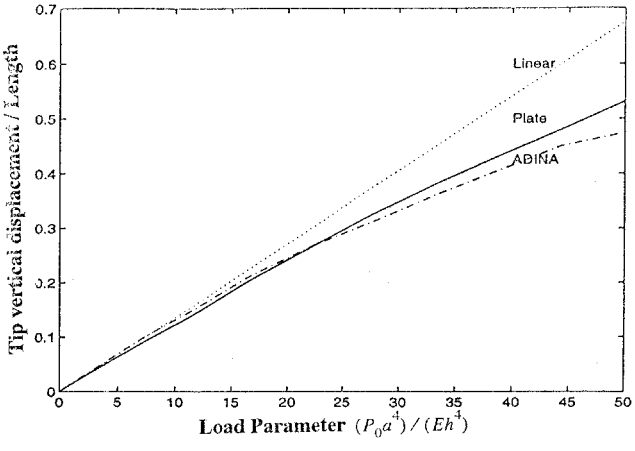

Fig. 5 Normalized tip vertical deflection, short cantilevered plate.

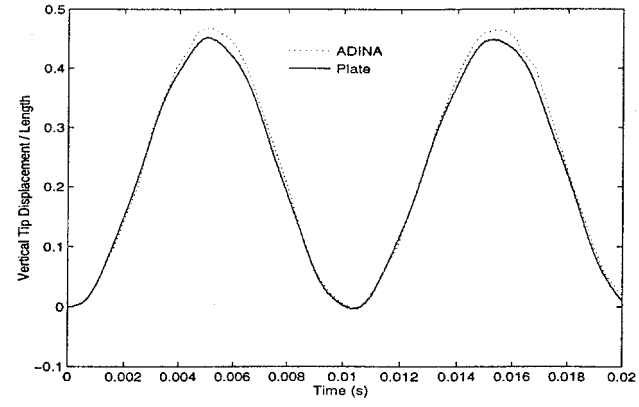

Fig. 6 Vertical tip deflection time response to 15-kPa uniform pressure step input, short cantilevered plate, linear stiffness.

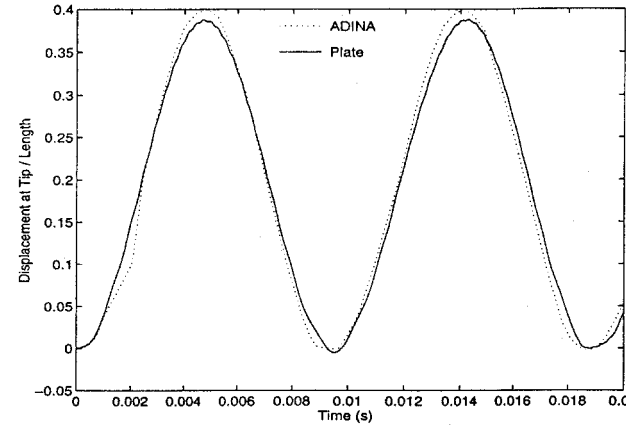

Fig. 7 Vertical tip deflection time response to 15-kPa uniform pressure step input, short cantilevered plate, nonlinear stiffness.

0.00948 s. The ADINA results showed a period of 0.0093 s. This represents about a 2% difference.

Results for Wing Box

The first results presented here are those corresponding to the static analysis. Six concentrated forces are applied to the wing box. One in-plane force is applied (its direction is parallel to the wing plane) to each of the front and rear spars caps (four in-plane forces in total). These in-plane forces are needed to compress the wing in-plane, such as can be expected in the case of the tail of a joined-wing airplane. In addition, two vertical forces are applied at the tip of the wing box, one in the plane of the web of the front spar and one in the plane of the web of the rear spar. For the examples presented here, all of the individual forces were set to have the same magnitude. This implies that the total in-plane load imposed on the structure is twice the total vertical load.

Before studying nonlinear effects, the linear solutions from ADINA and the equivalent plate methods developed here were compared. They were found to be very close, with a maximum difference of 4.5%. This can, of course, be expected because of slight differences in structural modeling assumptions between the two techniques. The ADINA model uses plate element for skins vs membranes in the equivalent plate approach. Small differences between the spar- and rib-web modeling in the equivalent plate approach and in the ADINA models can also lead to slight differences in results.

For the nonlinear static analysis, each of the forces mentioned earlier is progressively increased to obtain a displacement-load curve. Two cases were studied. In one, the loading forces stay fixed and do not change with the deformation. In the second case, the loading forces depend on deformation. Thus, when vertical deformation w is taken into account together with in-plane forces Px and Py, loading bending moments appear at the loaded wing tip and add to the loading on the wing. In Figs. 8 and 9, the displacement-load curves are presented for two different points along the tip of the wing box (the front and rear of the tip chord). The deformations were plotted against the total vertical load Pz (in the presence of the in-plane load). For presentation of results the applied load Pz was normalized by the wing-box length L, cross-sectional moment of inertia I, and the modulus of elasticity E, to produce the load parameter k $(=PzL^2/EI)$. It can be seen in Figs. 8 and 9 that the equivalent plate results match the finite element results very well up to a load parameter of about 0.25, even with fixed external loads. In general, the ADINA output shows larger deformations that those predicted by the present work with external fixed loads. When deformation-dependent loads were taken into account, correlation between the present equivalent plate results and the ADINA results is much improved. No computations beyond $k = 0.7$ were carried out because of the onset of yield.

Finally, nonlinear dynamic simulations were produced for the wing. With zero initial conditions, the loads (in-plane and vertical) were first increased from zero level up to a certain k-value level using a ramp that lasted 0.05 s. After that the loads were set constant

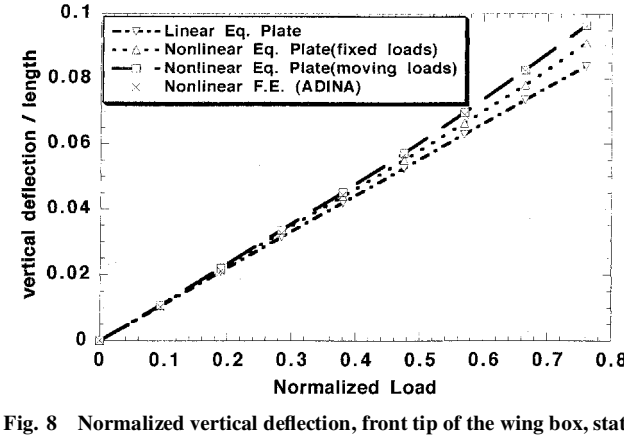

Fig. 8 Normalized vertical deflection, front tip of the wing box, static case.

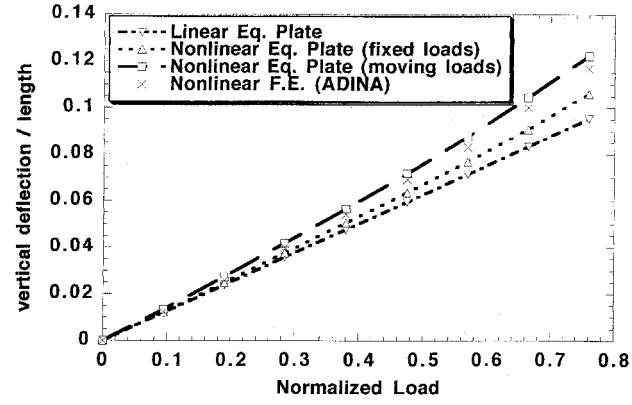

Fig. 9 Normalized vertical deflection, rear tip of the wing box, static case.

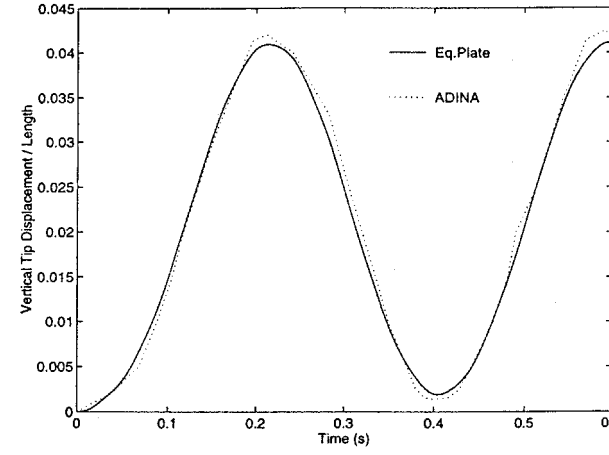

Fig. 10 Time response of vertical tip deflection to time-dependent load, $k = 0.19$.

for the remaining time. The results obtained using ADINA and the program developed here are shown in Fig. 10 for $k = 0.19$. Good correlation between the two outputs is observed, verifying the accuracy of the time integration used in the nonlinear equivalent plate capability. Good correlation with ADINA results had also been obtained deeper into the nonlinear response domain corresponding to higher loadings k.

Conclusions

A theory and an associated numerical analysis capability for the moderately large deformation nonlinear static and dynamic behavior of real wings loaded in-plane as well as perpendicular to their reference plane have been developed and discussed in this work. It was shown how linear equivalent plate modeling of wings made of composite cover skin and arrays of spars and ribs could be generalized and extended to cover nonlinear structural behavior due to moderately large deformations. Solution methods for the resulting static problems and for dynamic problems were described, and the new capability was evaluated by testing its performance using an array of test cases. These test cases contain a wing-box model, as well as full-depth plate and beam models. For the full-depth plate and beam cases, the new formulation (which was originally derived for skin/spar/rib wing boxes) had to be slightly modified.

Comparison of results from the new capability with results from the nonlinear structural analysis code ADINA on a number of cantilever plate and wing-box problems showed good correlation up to relatively large levels of loading. A series of test cases using simple beam models was used to gain experience with the number of terms needed for Ritz polynomials describing in-plane and out-of-plane motion. The capability to carry out buckling analysis and postbuckling analysis, and the capability to capture chaotic motion, were also verified using beam models.[18] Good results were obtained up to relatively large levels of loading.

Even though the capability developed herein is aimed at airplane wings, or wing/tail configurations, a few numerical tests were carried out to assess performance of the new capability for panels supported all around their circumference. This was done in an exploratory manner to take the new methodology to its limit, given the known ill-conditioning reached when the number of Ritz polynomial terms is too high, and the numerical difficulties associated with the need to impose boundary conditions via very stiff springs.

The new structural modeling approach for the moderately large deformation of wings offers fast and accurate structural capability for the nonlinear flutter analysis of geometrically nonlinear wing configurations. Aeroelastic analysis of such wings should then be the subject of research based on integration with unsteady lifting surface aerodynamics in the time domain, and using the time-integration techniques described in this work.

Appendix: *A*, *C*, *D*, *E* Matrices

[E_{ij}] Matrices

$$(1 \times N_{tu})[E_{11}] = \{\boldsymbol{a}_{1,x}\}^T$$

$$(1 \times N_{tw})[E_{13}] = -z \cdot \{\boldsymbol{a}_{3,xx}\}^T + \{\boldsymbol{q}_I\}^T \cdot \{\boldsymbol{a}_{I,x}\} \cdot \{\boldsymbol{a}_{3,x}\}$$

$$(1 \times N_{t\phi x})[E_{14}] = z \cdot \{\boldsymbol{a}_{4,x}\}^T, \qquad (1 \times N_{tv})[E_{22}] = \{\boldsymbol{a}_{2,y}\}^T$$

$$(1 \times N_{tw})[E_{23}] = -z \cdot \{\boldsymbol{a}_{3,yy}\}^T + \{\boldsymbol{q}_I\}^T \cdot \{\boldsymbol{a}_{I,y}\} \cdot \{\boldsymbol{a}_{3,y}\}$$

$$(1 \times N_{t\phi y})[E_{25}] = z \cdot \{\boldsymbol{a}_{5,y}\}^T, \qquad (1 \times N_{tu})[E_{31}] = \{\boldsymbol{a}_{1,y}\}^T$$

$$(1 \times N_{tv})[E_{32}] = \{\boldsymbol{a}_{2,x}\}^T$$

$$(1 \times N_{tw})[E_{33}] = -2z \cdot \{\boldsymbol{a}_{3,xy}\}^T + \{\boldsymbol{q}_I\}^T \cdot \{\boldsymbol{a}_{I,x}\} \cdot \{\boldsymbol{a}_{3,y}\} + \{\boldsymbol{q}_I\}^T \cdot \{\boldsymbol{a}_{I,y}\} \cdot \{\boldsymbol{a}_{3,x}\}^T$$

$$(1 \times N_{t\phi x})[E_{34}] = z \cdot \{\boldsymbol{a}_{4,y}\}^T, \qquad (1 \times N_{t\phi y})[E_{35}] = z \cdot \{\boldsymbol{a}_{5,x}\}^T$$

$$(N_{tw} \times N_{tw})[E_{16}] = \{\boldsymbol{a}_{3,x}\} \cdot \{\boldsymbol{a}_{3,x}\}^T$$

$$(N_{tw} \times N_{tw})[E_{26}] = \{\boldsymbol{a}_{3,y}\} \cdot \{\boldsymbol{a}_{3,y}\}^T$$

$$(N_{tw} \times N_{tw})[E_{36}] = 2\{\boldsymbol{a}_{3,x}\} \cdot \{\boldsymbol{a}_{3,y}\}^T$$

[A_{ij}] Matrices

$$[A_{11}] = Q_{11} \cdot E_{11} + Q_{16} \cdot E_{31}, \qquad [A_{12}] = Q_{12} \cdot E_{22} + Q_{16} \cdot E_{32}$$

$$[A_{13}] = Q_{11} \cdot E_{13} + Q_{12} \cdot E_{23} + Q_{16} \cdot E_{33}$$

$$[A_{14}] = Q_{11} \cdot E_{14} + Q_{16} \cdot E_{34}, \qquad [A_{15}] = Q_{12} \cdot E_{25} + Q_{16} \cdot E_{35}$$

$$[A_{21}] = Q_{21} \cdot E_{11} + Q_{26} \cdot E_{31}, \qquad [A_{22}] = Q_{22} \cdot E_{22} + Q_{26} \cdot E_{32}$$

$$[A_{23}] = Q_{21} \cdot E_{13} + Q_{22} \cdot E_{23} + Q_{26} \cdot E_{33}$$

$$[A_{24}] = Q_{21} \cdot E_{14} + Q_{26} \cdot E_{34}, \qquad [A_{25}] = Q_{22} \cdot E_{25} + Q_{26} \cdot E_{35}$$

$$[A_{31}] = Q_{61} \cdot E_{11} + Q_{66} \cdot E_{31}, \qquad [A_{32}] = Q_{62} \cdot E_{22} + Q_{66} \cdot E_{32}$$

$$[A_{33}] = Q_{61} \cdot E_{13} + Q_{62} \cdot E_{23} + Q_{66} \cdot E_{33}$$

$$[A_{34}] = Q_{61} \cdot E_{14} + Q_{66} \cdot E_{34}, \qquad [A_{35}] = Q_{62} \cdot E_{25} + Q_{66} \cdot E_{35}$$

[C_{ij}] Matrices

$$[C1]^T = Q_{11} \cdot E_{11}^T \cdot \{\boldsymbol{q}3\}^T \cdot E_{16} + Q_{16} \cdot E_{31}^T \cdot \{\boldsymbol{q}3\}^T \cdot E_{16} + Q_{21} \cdot E_{11}^T \cdot \{\boldsymbol{q}3\}^T \cdot E_{26} + Q_{26} \cdot E_{31}^T \cdot \{\boldsymbol{q}3\}^T \cdot E_{26} + Q_{61} \cdot E_{11}^T \cdot \{\boldsymbol{q}3\}^T \cdot E_{36} + Q_{66} \cdot E_{31}^T \cdot \{\boldsymbol{q}3\}^T \cdot E_{36}$$

$$[C2]^T = Q_{12} \cdot E_{22}^T \cdot \{\boldsymbol{q}3\}^T \cdot E_{16} + Q_{16} \cdot E_{32}^T \cdot \{\boldsymbol{q}3\}^T \cdot E_{16} + Q_{22} \cdot E_{22}^T \cdot \{\boldsymbol{q}3\}^T \cdot E_{26} + Q_{26} \cdot E_{32}^T \cdot \{\boldsymbol{q}3\}^T \cdot E_{26} + Q_{62} \cdot E_{22}^T \cdot \{\boldsymbol{q}3\}^T \cdot E_{36} + Q_{66} \cdot E_{32}^T \cdot \{\boldsymbol{q}3\}^T \cdot E_{36}$$

$$[C3] = Q_{11} \cdot E_{16}^T \cdot \{\boldsymbol{q}3\} \cdot E_{13} + Q_{12} \cdot E_{16}^T \cdot \{\boldsymbol{q}3\} \cdot E_{23} + Q_{16} \cdot E_{16}^T \cdot \{\boldsymbol{q}3\} \cdot E_{33} + Q_{12} \cdot E_{26}^T \cdot \{\boldsymbol{q}3\} \cdot E_{13} + Q_{22} \cdot E_{26}^T \cdot \{\boldsymbol{q}3\} \cdot E_{23} + Q_{26} \cdot E_{26}^T \cdot \{\boldsymbol{q}3\} \cdot E_{33} + Q_{16} \cdot E_{36}^T \cdot \{\boldsymbol{q}3\} \cdot E_{13} + Q_{26} \cdot E_{36}^T \cdot \{\boldsymbol{q}3\} \cdot E_{23} + Q_{66} \cdot E_{36}^T \cdot \{\boldsymbol{q}3\} \cdot E_{33}$$

$$[C4] = Q_{11} \cdot E_{16}^T \cdot \{\boldsymbol{q}3\} \cdot E_{14} + Q_{16} \cdot E_{16}^T \cdot \{\boldsymbol{q}3\} \cdot E_{34} + Q_{12} \cdot E_{26}^T \cdot \{\boldsymbol{q}3\} \cdot E_{14} + Q_{26} \cdot E_{26}^T \cdot \{\boldsymbol{q}3\} \cdot E_{34} + Q_{16} \cdot E_{36}^T \cdot \{\boldsymbol{q}3\} \cdot E_{14} + Q_{66} \cdot E_{36}^T \cdot \{\boldsymbol{q}3\} \cdot E_{34}$$

$$[C5] = Q_{12} \cdot E_{16}^T \cdot \{\boldsymbol{q}3\} \cdot E_{25} + Q_{16} \cdot E_{16}^T \cdot \{\boldsymbol{q}3\} \cdot E_{35} + Q_{22} \cdot E_{26}^T \cdot \{\boldsymbol{q}3\} \cdot E_{25} + Q_{26} \cdot E_{26}^T \cdot \{\boldsymbol{q}3\}^T \cdot E_{35} + Q_{62} \cdot E_{36}^T \cdot \{\boldsymbol{q}3\} \cdot E_{25} + Q_{66} \cdot E_{36}^T \cdot \{\boldsymbol{q}3\} \cdot E_{35}$$

Matrix [D]

$$[D] = Q_{11} \cdot E_{16}^T \cdot \{\boldsymbol{q}3\} \cdot \{\boldsymbol{q}3\}^T \cdot E_{16} + Q_{12} \cdot E_{16}^T \cdot \{\boldsymbol{q}3\} \cdot \{\boldsymbol{q}3\}^T \cdot E_{26} + Q_{16} \cdot E_{16}^T \cdot \{\boldsymbol{q}3\} \cdot \{\boldsymbol{q}3\}^T \cdot E_{36} + Q_{12} \cdot E_{26}^T \cdot \{\boldsymbol{q}3\} \cdot \{\boldsymbol{q}3\}^T \cdot E_{16} + Q_{22} \cdot E_{26}^T \cdot \{\boldsymbol{q}3\} \cdot \{\boldsymbol{q}3\}^T \cdot E_{26} + Q_{26} \cdot E_{26}^T \cdot \{\boldsymbol{q}3\} \cdot \{\boldsymbol{q}3\}^T \cdot E_{36} + Q_{16} \cdot E_{36}^T \cdot \{\boldsymbol{q}3\} \cdot \{\boldsymbol{q}3\}^T \cdot E_{16} + Q_{26} \cdot E_{36}^T \cdot \{\boldsymbol{q}3\} \cdot \{\boldsymbol{q}3\}^T \cdot E_{26} + Q_{66} \cdot E_{36}^T \cdot \{\boldsymbol{q}3\} \cdot \{\boldsymbol{q}3\}^T \cdot E_{36}$$

Acknowledgment

This research was funded by the National Science Foundation through a National Young Investigator grant. This support is gratefully acknowledged.

References

[1]Turner, C. D., and Ricketts, R. H., "Aeroelastic Considerations for Continuous Patrol/High Altitude Surveillance Platform," AIAA Paper 83-0924, May 1983.

[2]Gallman, J. W., and Kroo, I. M., "Structural Optimization for Joined-Wing Synthesis," *Journal of Aircraft*, Vol. 33, No. 1, 1996, pp. 214–223.

[3]Bathe, K.-J., *Finite Element Procedures*, Prentice–Hall, Englewood Cliffs, NJ, 1996.

[4]Lynch, R. W., Rogers, W. A., and Brayman, W. W., "Aeroelastic Tailoring of Advanced Composite Structures for Military Aircraft," U.S. Air Force Flight Dynamics Lab., AFFDL-TR-76-100, Wright-Patterson AFB, OH, April 1977.

[5]Triplett, W. E., "Aeroelastic Tailoring Studies in Fighter Aircraft Design," *Journal of Aircraft*, Vol. 17, No. 7, 1980, pp. 508–513.

[6]Giles, G. L., "Equivalent Plate Analysis of Aircraft Wing Box Structures with General Planform Geometry," *Journal of Aircraft*, Vol. 23, No. 11, 1986, pp. 859–864.

[7]Giles, G. L., "Further Generalization of an Equivalent Plate Representation for Aircraft Structural Analysis," *Journal of Aircraft*, Vol. 26, No. 1, 1989, pp. 67–74.

[8]Livne, E., Schmit, L. A., and Friedmann, P., "Design Oriented Structural Analysis for Fiber Composite Wings," Mechanical, Aerospace and Nuclear Engineering Dept., Univ. of California, UCLA-ENG-88-36, Los Angeles, CA, Nov. 1988.

[9]Livne, E., "Integrated Multidisciplinary Optimization of Actively Controlled Fiber Composite Wings," Ph.D. Dissertation, Mechanical, Aerospace and Nuclear Engineering Dept., Univ. of California, Los Angeles, CA, 1990.

[10]Livne, E., "Equivalent Plate Structural Modeling for Wing Shape Optimization Including Transverse Shear," *AIAA Journal*, Vol. 32, No. 6, 1994, pp. 1278–1288.

[11]Livne, E., Sels, R. A., and Bhatia, K. G., "Lessons from Application of Equivalent Plate Structural Modeling to an HASCT Wing," *Journal of Aircraft*, Vol. 31, No. 4, 1994, pp. 953–960.

[12]Livne, E., "Analytic Sensitivities for Shape Optimization in Equivalent Plate Structural Wing Models," *Journal of Aircraft*, Vol. 31, No. 4, 1994, pp. 961–969.

[13]Borchert, R. Q., "Improvements in Design Oriented Equivalent Plate Modeling of Wing Structures," M.S. Thesis, Dept. of Aeronautics and Astronautics, Univ. of Washington, Seattle, WA, 1995.

[14]Giles, G. L., "Equivalent Plate Modeling of Conceptual Design of Aircraft Wing Structures," AIAA Paper 95-3945, Sept. 1995.

[15]Livne, E., and Milosavljevic, R., "Analytic Sensitivity and Approximation of Skin Buckling Constraints in Wing-Shape Synthesis," *Journal of Aircraft*, Vol. 32, No. 5, 1995, pp. 1102–1113.

[16]Reddy, J. N., *Energy and Variational Methods in Applied Mechanics*, Wiley, New York, 1984, Chap. 4.

[17]Chia, C.-Y., *Nonlinear Analysis of Plates*, McGraw–Hill, New York, 1980.

[18]Navarro, I., "Nonlinear Equivalent Plate Modeling of Wing Structures," M.S. Thesis, Dept. of Aeronautics and Astronautics, Univ. of Washington, Seattle, WA, 1997.

[19]Dugundji, J., Minguet, P. J., and Lagace, P., "Postbuckling Behavior of Laminated Plates Using a Direct Energy-Minimization Technique," *AIAA Journal*, Vol. 27, No. 12, 1989, pp. 1785–1792.

[20]Livne, E., and Navarro, I., "Nonlinear Equivalent Plate Modeling of Wing Box Structures," AIAA Paper 99-1234, April 1999.

[21]Argyris, J., and Mlejenk, H.-P., *Dynamics of Structures*, North–Holland, Amsterdam, 1991, Chap. 11.

[22]Moorthy, R. I. K., and Kakodkar, H. R., "An Assessment of the Newmark Method for Solving Chaotic Vibrations of Impacting Oscillators," *Computers and Structures*, Vol. 49, No. 4, 1993, pp. 597–603.

[23]Whitney, J. M., "Stress Analysis of Thick Laminated Composite and Sandwich Plates," *Journal of Composite Materials*, Vol. 6, Oct. 1972, pp. 426–441.

[24]*ADINA: Theory and Modeling Guide*, ADINA R&D, Inc., Watertown, MA, 1995.